Envelope-function formalism for phonons in heterostructures

Hiroshi Akera and Tsuneya Ando
Institute for Solid State Physics, University of Tokyo, 7-22-1 Roppongi, Minato-ku, Tokyo 106, Japan
(Received 16 November 1988; revised manuscript received 17 April 1989)

An envelope-function formalism analogous to the effective-mass theory for electrons is developed to treat long-wavelength phonons in semiconductor heterostructures. It consists of a set of differential equations for phonon envelope functions and their boundary conditions at interfaces. For acoustic phonons the present theory becomes equivalent to the elasticity theory. For optical phonons there are two cases to which our formalism is applicable. In the first case, in which the bulk optical bands of constituent materials overlap considerably, as in InAs/GaSb and GaAs/Ge, the boundary conditions are written in the form of linear relations among envelopes and their derivatives on both sides of the interface. The boundary conditions strongly depend not only on the materials but also on the atomic configuration at interfaces. In the second case, where there is a large gap between the bulk optical branches, as in GaAs/AlAs, the boundary conditions that the envelopes should vanish at interfaces are generally appropriate.

I. INTRODUCTION

The nature of optical phonons is strongly modified in semiconductor heterostructures such as quantum wells and superlattices.[1] Some phonons are confined in one of the layers, and some are localized around the interface. The purpose of this paper is to construct a continuum formalism for optical phonons in heterostructures that properly describes the boundary conditions at the interface.

Our formalism is an extension of the effective-mass theory[2] for electrons to the phonon problem. The effective-mass formalism is, although quite simple, a well-established and powerful method for describing electron motions in the vicinity of band extrema. Although there are many other methods for the calculation of band structure, such as the first-principles calculation, the empirical pseudopotential method, and the tight-binding model, their complexity prevents wide application, including calculations of effects of electron-phonon interactions, leading to the present situation that the effective-mass formalism still remains the most widely used method. Our formalism for phonons aims at this kind of usefulness, especially in the calculation of the electron-phonon interaction.

Another feature of our formalism is to describe the behavior of phonon modes in the vicinity of an interface as a compact boundary condition. In this respect it is useful to refer to the studies on the connection rule of electron envelope functions in the effective-mass theory.[3-10] It has been known that the so-called envelope-function approximation works surprisingly well in heterostructures consisting of GaAs and AlAs. In the envelope-function approximation, the envelope itself is continuous, but its derivative is discontinuous in such a way that the current conservation is satisfied across the interface. However, this approximation is not necessarily applicable to the other heterostructures. To express the general connection rule, the interface matrix has been introduced.[3] Consider the interface at $z=0$ of two semiconductors A ($z<0$) and B ($z>0$). The connection rule for electrons in a single-band minimum is generally expressed as the following linear equations for envelopes ζ and their derivatives:

$$\begin{bmatrix} \zeta_B \\ \nabla\zeta_B \end{bmatrix} = T_{BA} \begin{bmatrix} \zeta_A \\ \nabla\zeta_A \end{bmatrix}, \tag{1.1}$$

where $T_{BA}=(t_{ij})$ is a 2×2 interface matrix and $\nabla=(a/4)(\partial/\partial z)$, with a the lattice constant [$\nabla=a(\partial/\partial z)$ in Ref. 3]. The envelope-function approximation corresponds to the interface matrix given by $t_{11}=1$, $t_{12}=t_{21}=0$, and $t_{22}=m_B/m_A$, where m_A and m_B are the effective masses. The interface matrix expresses an effect of the interface by specifying a condition for the behavior of wave functions sufficiently away from the interface. Also, in the case of phonons the calculation of such an interface matrix can serve for the understanding of the effect of the existence of an interface on the behavior of phonon modes.

It is worthwhile to briefly review the existing methods for the calculation of phonon eigenmodes to clarify the standing of our formalism. The most standard method is to solve the equations of motion for the displacements of atoms by diagonalizing the dynamical matrix. Several authors have calculated phonon modes in superlattices within a linear-chain model.[11-15] This model can only describe phonon modes of perpendicular propagation, i.e., modes whose wave vectors are perpendicular to interfaces. Recently, the calculation was extended to phonons of nonperpendicular propagation, using the shell model[16] and the rigid-ion model.[17,18]

However, the results of such calculations are not useful for investigation of the Fröhlich-type electron-phonon interaction, because phonon modes are expressed by displacements of each atom. If we are to calculate the matrix elements of the Fröhlich Hamiltonian within the effective-mass theory, we need the polarization $\mathbf{P}(\mathbf{r})$ due

to optical phonons as a continuous function of spatial coordinate **r**. Since long-wavelength optical phonons make a main contribution to the Fröhlich interaction, a continuum model is highly required.

The dielectric continuum model has been widely used in heterostructures[19–22] and slabs.[23–25] The phonons in this model are the Einstein modes coupled only by dipole-dipole interactions. The model neglects the short-range interactions between the modes, leading to the result that frequencies of all modes in heterostructures are degenerate at bulk values of zero wave number, except the Fuchs-Kliewer modes. The Fuchs-Kliewer modes, for example, in superlattices exhibit a characteristic angular dispersion at the Γ point, i.e., the dependence of frequency on the direction of wave vector, due to the anisotropy of the macroscopic electric field produced by the polarization.

There have been some attempts to generalize the dielectric continuum model so as to take into account effects of the dispersion and the boundary condition. Mills[26] investigated longitudinal-optical (LO) phonons of perpendicular propagation in depletion layers on semiconductor surfaces, assuming that the envelope, i.e., the relative displacement of a cation and an anion in a unit cell, has a vanishing derivative at the surface. Babiker[27] proposed an isotropic model for LO phonons in $GaAs/Al_{1-x}Ga_xAs$ alloy heterostructures. In this model, he used hydrodynamic boundary conditions at interfaces, which neglect mixings of LO and TO (transverse optical) modes completely. Quite recently, Chu, Ren, and Chang[28] combined a linear-chain model with the dielectric continuum model in order to describe the angular dispersion of optical phonons at the Γ point in GaAs/AlAs superlattices.

In the present paper we construct a more complete continuum model for long-wavelength phonons in heterostructures, starting with lattice dynamics. Phonons are described by envelopes that are a vector with three components corresponding to x, y, and z displacements and that satisfy a set of coupled differential equations. Effects of an interface are taken into account in the form of boundary conditions for these envelopes. The boundary conditions are derived from the equations of motion near the interface. For acoustic modes, the boundary conditions turn out to be equivalent to those of the elasticity theory, as might be expected, i.e., that the displacement and the stress should be continuous across the interface.[29] In the case of optical modes, there is always a difference in bulk frequencies at zero wave number of the constituent semiconductors, which produces a steplike "potential" corresponding to band offsets for electrons. The present envelope-function formalism is applicable to the following two cases: the case that this band offset is much smaller than the bandwidth in the bulk, and the case that it is sufficiently larger than the bandwidth. In the former case, displacements in both sides of the interface are well described by envelopes, and the boundary conditions are expressed by a 6×6 interface matrix. Typical examples are InAs/GaSb and GaAs/Ge heterostructures. In the latter case, whose most typical example is GaAs/AlAs, phonons are well confined in each material, and appropriate boundary conditions for envelopes are such that they should vanish on a certain plane parallel to the interface.

The organization of the present paper is as follows. First, we consider the case that envelopes can be defined at the same time in both sides of an interface. In Sec. II the envelope-function formalism is derived, as an illustration, in a simple linear-chain model.[30] The envelope functions for acoustic and optical modes are defined, and the differential equations and interface matrices are derived. In Sec. III the formalism is generalized to optical phonons with the wave vector in arbitrary directions. To obtain explicit results, a simple valence-force-field model is used, although the calculation using more refined models is straightforward. In spite of its simplicity, the valence-force-field model reproduces the observed bulk dispersion relation well. In Sec. IV the present formalism is applied to InAs/GaSb and GaAs/Ge superlattices, and the results are compared with those by the dielectric continuum model. Next, optical phonons in GaAs/AlAs systems are discussed, and the boundary conditions are derived in Sec. V. The summary and conclusions are given in Sec. VI.

The envelope-function formalism can be extended to various other cases. The formalism for the modes near the Brillouin-zone boundary along the [001] direction (X point) is given in Appendix A, and the connection rules for the GaAs heterostructure, in which one Ga atomic plane is replaced by an Al or In plane, are given in Appendix B. In Appendix C the conditions for interface matrices are obtained from the energy-conservation law. In Appendix D some symmetry relations of interface matrices are derived. In Appendix E the explicit results are presented for zinc-blende structure with use of the valence-force-field model. In Appendix F the procedure is given for the calculation of interface matrices in the presence of second-neighbor forces.

II. LINEAR-CHAIN MODEL

A. Differential equation in the bulk

Modes with wave vector parallel to the [001] crystal axis of zinc-blende structure can be described by the linear-chain model shown in Fig. 1. There are two atoms in a unit cell: a cation (positive ion) and an anion (negative ion) whose masses are denoted M_c and M_a, respectively. The distance a_0 between adjacent atomic planes is $a/4$, where a is the lattice constant. We choose the z axis along the chain direction and the other axes x, y, ξ, and η along [100], [010], [$1\bar{1}0$], and [110] crystal axes, respectively, as defined in Fig. 2. We denote modes with displacements along each of the ξ, η, and z directions by ξ, η, and z modes, respectively. The z modes are longitudinal, and the others are transverse. They are decoupled from each other due to the reflection symmetry of the zinc-blende structure. We restrict ourselves to nearest-neighbor forces in this section, and the effects of long-range Coulomb forces are discussed in the next section. For z modes, the force constants f_1 and f_2 in Fig. 1 are the same, whereas they are different for ξ and η modes.

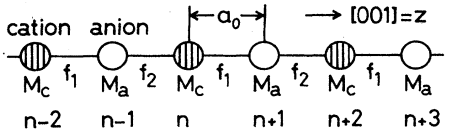

FIG. 1. Linear-chain model for the bulk with only first-neighbor force constants f_1 and f_2. For displacements along the z axis, $f_1=f_2$, whereas $f_1\neq f_2$ for those along the ξ and η axes. The masses of the cation and anion are denoted by M_c and M_a, respectively.

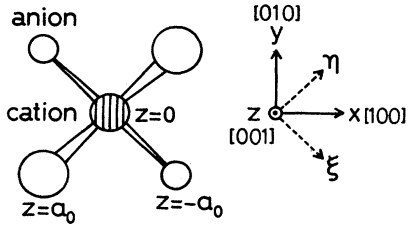

FIG. 2. Definition of axes. Top view from [001].

These force constants are expressed in Appendix E by the valence-force-field parameters introduced in Sec. III B. We consider here modes near the Γ point and those near the X point in Appendix A.

We start with the dynamical matrix for the bulk crystal. Consider modes with displacements

$$u_c(z_n)=u_c(k)e^{ikz_n-i\omega t},\qquad u_a(z_m)=u_a(k)e^{ikz_m-i\omega t}, \tag{2.1}$$

for a cation at z_n and an anion at z_m, where $z_n=na_0$. The dynamical equation is

$$D_u(k)\begin{bmatrix}(M_c)^{1/2}u_c(k)\\(M_a)^{1/2}u_a(k)\end{bmatrix}=\omega^2\begin{bmatrix}(M_c)^{1/2}u_c(k)\\(M_a)^{1/2}u_a(k)\end{bmatrix}. \tag{2.2}$$

The dynamical matrix D_u is given by

$$D_u(k)=\frac{\omega_{\rm TO}^2}{r_m+r_m^{-1}}\begin{bmatrix}r_m & -[Fe^{ika_0}+(1-F)e^{-ika_0}]\\ -[Fe^{-ika_0}+(1-F)e^{ika_0}] & r_m^{-1}\end{bmatrix}, \tag{2.3}$$

with

$$\omega_{\rm TO}^2=\frac{f_1+f_2}{M_r},\quad F=\frac{f_1}{f_1+f_2},\quad r_m=\left[\frac{M_a}{M_c}\right]^{1/2}, \tag{2.4}$$

where M_r is the reduced mass given by $M_cM_a/(M_c+M_a)$. Any eigenvector is expressed as a linear combination of two eigenvectors at $k=0$:

$$\begin{bmatrix}(M_c)^{1/2}u_c(k)\\(M_a)^{1/2}u_a(k)\end{bmatrix}=\frac{1}{N}\begin{bmatrix}1 & r_m\\ r_m & -1\end{bmatrix}\begin{bmatrix}w_\alpha(k)\\w_\beta(k)\end{bmatrix}, \tag{2.5}$$

where $N=(1+r_m^2)^{1/2}$. In the long-wavelength limit the dynamical matrix for the expansion coefficients $w_\alpha(k)$ and $w_\beta(k)$ is

$$D_w(k)=\frac{\omega_{\rm TO}^2}{r_+}\begin{bmatrix}\frac{1}{r_+}(ka_0)^2 & (2F-1)ika_0\\ -(2F-1)ika_0 & r_+-\frac{1}{r_+}(ka_0)^2\end{bmatrix}, \tag{2.6}$$

where

$$r_+=r_m+r_m^{-1}. \tag{2.7}$$

Here we have retained the terms up to the second order of ka_0 for diagonal elements and those up to the first order for off-diagonal elements. The above matrix corresponds to the $k\cdot p$ Hamiltonian in the electron problem. The $k\cdot p$ terms disappear for z modes since $f_1=f_2$.

To diagonalize $D_w(k)$, we perform the following unitary transformation:

$$\begin{bmatrix}w_\alpha(k)\\w_\beta(k)\end{bmatrix}=e^S\begin{bmatrix}\phi_{\rm ac}(k)\\\phi_{\rm op}(k)\end{bmatrix}, \tag{2.8}$$

where the requirement that the terms linear in ka_0 vanish in $e^{-S}D_we^S$ gives

$$S=\begin{bmatrix}0 & \gamma ika_0\\ \gamma ika_0 & 0\end{bmatrix}, \tag{2.9}$$

with $\gamma=(2F-1)/r_+$. The diagonalized Hamiltonian is

$$D_\phi(k)=\frac{\omega_{\rm TO}^2}{r_+}\begin{bmatrix}\frac{1}{r_+}[1-(2F-1)^2](ka_0)^2 & 0\\ 0 & r_+-\frac{1}{r_+}[1-(2F-1)^2](ka_0)^2\end{bmatrix}. \tag{2.10}$$

In the real-space representation we obtain second-order differential equations:

$$\omega^2 U(z) = -\alpha_0 \nabla^2 U(z) \tag{2.11}$$

and

$$(\omega^2 - \omega_{\rm TO}^2) u(z) = -\alpha_1 \nabla^2 u(z) , \tag{2.12}$$

with $\nabla = a_0(\partial/\partial z)$, where

$$\alpha_0 = -\alpha_1 = \left[\frac{\omega_{\rm TO}}{r_+}\right]^2 [1-(2F-1)^2] . \tag{2.13}$$

The envelope functions $U(z)$ and $u(z)$ are those for acoustic and optical modes, respectively, and are defined by

$$\begin{aligned} U(z) &= [M_c(1+r_m^2)]^{-1/2} \phi_{\rm ac}(z) \\ u(z) &= \left[\frac{1+r_m^2}{M_a}\right]^{1/2} \phi_{\rm op}(z) . \end{aligned} \tag{2.14}$$

The above differential equations correspond to the effective-mass equation for electrons. The "effective mass" is the same for acoustic and optical modes, except the sign, and it is larger for transverse modes ($F \neq \frac{1}{2}$) than for longitudinal modes ($F = \frac{1}{2}$). The relation between the envelope functions and the displacements is

$$\begin{bmatrix} u_c(k) \\ u_a(k) \end{bmatrix} = \begin{bmatrix} 1 & r_m \\ 1 & -r_m^{-1} \end{bmatrix} \begin{bmatrix} 1 & \gamma i k a_0 \\ \gamma i k a_0 & 1 \end{bmatrix} \begin{bmatrix} 1 & 0 \\ 0 & r_+^{-1} \end{bmatrix} \begin{bmatrix} U(k) \\ u(k) \end{bmatrix} , \tag{2.15}$$

which reduces to $U = u_c = u_a$ and $u = u_c - u_a$ when $k = 0$.

B. Connection rule

Consider heterostructures in which the difference between the bulk frequencies at zero wave number of the constituent materials is small compared to the width of the band considered. The envelopes in both sides of an interface satisfy a second-order differential equation. The connection rule for such envelopes is in general expressed by an interface matrix:

$$\begin{bmatrix} \zeta_B \\ \nabla \zeta_B \end{bmatrix} = T_{BA} \begin{bmatrix} \zeta_A \\ \nabla \zeta_A \end{bmatrix}, \quad T_{BA} = \begin{bmatrix} t_{11} & t_{12} \\ t_{21} & t_{22} \end{bmatrix} , \tag{2.16}$$

where $\nabla = a_0(\partial/\partial z)$. The envelope function $\zeta(z)$ is $U(z)$ for acoustic modes and $u(z)$ for optical modes. The interface matrix must satisfy the condition of the energy conservation described in Appendix C. The roles of t_{11} and t_{22} are obvious: they connect the envelope functions and their derivatives, respectively. The off-diagonal elements t_{21} and t_{12} also have a clear meaning. Let us consider the case that $t_{11} = t_{22} = 1$ and $t_{12} = 0$. The effect of t_{21} corresponds to the presence of the δ-function potential[6] $\alpha_i a_0 t_{21} \delta(z)$ $(i = 0, 1)$ in the differential equations (2.11) and (2.12), where α_i is the prefactor in the dispersion term. When t_{21} is positive (negative), the absolute value of the envelope function shows a downward (upward) cusp at the interface because of a repulsive (attractive) potential. A localized interface mode always exists when t_{21} is negative. When $|t_{21}| \gg 1$, the magnitude of the envelope function is vanishingly small, except the above localized mode. Next we consider the case that $t_{11} \neq t_{22}$ and $t_{21} = 0$ to examine the role of t_{12}. The connection rule can be expressed by using the envelope functions at the displaced position $z = \epsilon a_0$. The interface matrix is now modified to $t'_{12} = t_{12} + (t_{22} - t_{11})\epsilon$, with the other elements unchanged. By choosing an appropriate value of ϵ, we can make t'_{12} vanish, showing that the effect of t_{12} is to change the interface position. When t_{12} is extremely large, however, the connection rule is such that the derivative of the envelope function vanishes.

We consider the connection rule at the interface consisting of a cation in A and an anion in B as shown in Fig. 3. The connection rule for another atomic configuration can be obtained using the symmetry relation described in Appendix D. We present the interface matrices for modes near the X point in Appendix A and those for the GaAs heterostructure in which all the Ga atoms in a plane are replaced by Al or In in Appendix B.

The equations of motion in the vicinity of the interface are

$$\begin{aligned} -\omega^2 M_{cA} u_{cA}(n) &= -f_{2A}[u_{cA}(n) - u_{aA}(n-1)] \\ &\quad - f_{1I}[u_{cA}(n) - u_{aB}(n+1)] , \\ -\omega^2 M_{aB} u_{aB}(n+1) &= -f_{1I}[u_{aB}(n+1) - u_{cA}(n)] \\ &\quad - f_{2B}[u_{aB}(n+1) - u_{cB}(n+2)] , \end{aligned} \tag{2.17}$$

where M_{cA} and M_{aB} are the masses of a cation in A and an anion in B, u_{cA} and u_{aB} are corresponding displacements, and f_{2A}, f_{1I}, and f_{2B} are the first-neighbor force constants shown in Fig. 3. Taking the difference between the above equations and those for the bulk, we get a relation between displacements:

$$\begin{bmatrix} 0 & f_{1I} \\ f_{1B} & f_{1I} - f_{1B} \end{bmatrix} \begin{bmatrix} u_{cB}(n) \\ u_{aB}(n+1) \end{bmatrix} = \begin{bmatrix} f_{1I} - f_{1A} & f_{1A} \\ f_{1I} & 0 \end{bmatrix} \begin{bmatrix} u_{cA}(n) \\ u_{aA}(n+1) \end{bmatrix} . \tag{2.18}$$

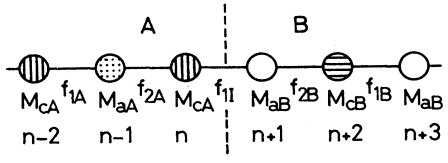

FIG. 3. Linear-chain model for a single heterostructure with only first-neighbor force constants f_1 and f_2.

The displacements are expressed in terms of the envelope functions according to Eq. (2.15):

$$\begin{bmatrix} u_c(n) \\ u_a(n+1) \end{bmatrix} = \begin{bmatrix} 1 & r_m\gamma - \frac{1}{2} \\ 1 & -r_m^{-1}\gamma + \frac{1}{2} \end{bmatrix} \begin{bmatrix} U \\ \nabla U \end{bmatrix}, \tag{2.19}$$

for acoustic modes, and

$$\begin{bmatrix} u_c(n) \\ u_a(n+1) \end{bmatrix} = \frac{1}{r_+} \begin{bmatrix} r_m & \gamma - \frac{1}{2}r_m \\ -r_m^{-1} & \gamma - \frac{1}{2}r_m^{-1} \end{bmatrix} \begin{bmatrix} u \\ \nabla u \end{bmatrix}, \tag{2.20}$$

for optical modes, where $\gamma = (2F-1)/r_+$ and $r_+ = r_m + r_m^{-1}$.

For acoustic modes, the interface matrix is obtained as

$$t_{11} = 1, \quad t_{21} = 0, \tag{2.21}$$

$$t_{12} = \frac{1}{2(1-F_B)} \left[\gamma_A \gamma_B \left(\frac{r_{mB}}{r_{mA}} - \frac{r_{mA}}{r_{mB}} \right) + \tfrac{1}{2}\gamma_A (r_{mA} - r_{mA}^{-1}) - \tfrac{1}{2}\gamma_B (r_{mB} - r_{mB}^{-1}) \right] + \left[\frac{f_{1A}}{f_{1B}} - 1 \right] \frac{1-F_A}{1-F_B} (\tfrac{1}{2} - r_{mB}\gamma_B) + 2f_{1A}(f_{1I}^{-1} - f_{1B}^{-1})(1-F_A), \tag{2.22}$$

$$t_{22} = \frac{(M_{cA} + M_{aA})v_A^2}{(M_{cB} + M_{aB})v_B^2}, \tag{2.23}$$

where v is the sound velocity for the mode considered. When $\gamma = 0$ (z modes) and $f_{1A} = f_{1B} = f_{1I}$, we have $t_{12} = 0$. And, as will be shown in Table II, t_{12} is smaller than unity in the case of InAs/GaSb and GaAs/Ge interfaces, giving the change of interface position less than the lattice constant. Therefore our connection rule is equivalent to that of the elasticity theory: the displacement and the stress are continuous across the interface.

Next, we discuss the connection rule for optical modes. We present the formula of the interface matrix only for z modes for which $\gamma = 0$:

$$T_{BA} = T_{BA0} + \left[1 - \frac{f_{1A}}{f_{1B}} \right] T_{BA1} + f_{1A}(f_{1B}^{-1} - f_{1I}^{-1}) T_{BA2}, \tag{2.24}$$

where

$$T_{BA0} = \frac{r_{+B}}{r_{+A}} \begin{bmatrix} \frac{1}{2}(R_m + R_m^{-1}) & \frac{1}{4}(R_m - R_m^{-1}) \\ R_m - R_m^{-1} & \frac{1}{2}(R_m + R_m^{-1}) \end{bmatrix}, \tag{2.25}$$

$$T_{BA1} = \frac{r_{+B}}{r_{+A}} \begin{bmatrix} -\frac{1}{2}r_{+A}r_{mB} & \frac{1}{4}r_{-A}r_{mB} \\ -r_{+A}r_{mB} & \frac{1}{2}r_{-A}r_{mB} \end{bmatrix}, \tag{2.26}$$

and

$$T_{BA2} = \frac{r_{+B}}{r_{+A}} \begin{bmatrix} -\frac{1}{2}r_{+A}r_{-B} & \frac{1}{4}r_{-A}r_{-B} \\ -r_{+A}r_{+B} & \frac{1}{2}r_{-A}r_{+B} \end{bmatrix}. \tag{2.27}$$

Here, $R_m = r_{mB}/r_{mA}$, $r_+ = r_m + r_m^{-1}$, and $r_- = r_m - r_m^{-1}$. Most III-V compound semiconductors with zinc-blende structure have almost same force constants, and the variety of lattice dynamics comes mainly from the differences in the masses of ions. Neglecting the small differences between force constants f_{1A}, f_{1B}, and f_{1I}, we get $T_{BA} = T_{BA0}$. The key element t_{21} in T_{BA} depends strongly on the difference in the mass ratio M_a/M_c of the two materials. As a matter of fact, we have $t_{21} \sim 1$ for InAs(A)/GaSb(B) and $t_{21} \sim 0$ for GaAs(A)/Ge(B).

Babiker[27] proposed a connection rule for LO modes, which corresponds to the interface matrix: $t_{11} = 1$, $t_{21} = t_{12} = 0$, and $t_{22} = \rho_{rA}v_A^2/\rho_{rB}v_B^2$, where ρ_r is the reduce mass density and v is the sound velocity, and applied it to GaAs/$Al_{1-x}Ga_xAs$ alloy heterostructures. This connection rule is analogous to that of the elasticity theory and is the simplest one that satisfies the energy-conservation law (Appendix C). However, our calculation shows that it is not in general valid, but may be applicable to optical modes in GaAs/Ge heterostructures (Sec. IV A) and some modes near the X point (Appendix A).

III. THREE-DIMENSIONAL LATTICE DYNAMICS

A. Differential equation and connection rule

We now extend the formalism to optical phonons with wave vector in arbitrary directions. As in the case of the linear-chain model considered in the preceding section, we derive the equation for the envelope function starting from the dynamical matrix. The procedure is straightforward and the envelope, expressed by a vector $\mathbf{u} = (u_x, u_y, u_z)$, now satisfies a matrix Schrödinger-type equation, which in crystals with zinc-blende or cubic symmetry takes the form

$$(\omega^2 - \omega_{\mathrm{TO}}^2)\mathbf{u}(\mathbf{k}) = H(\mathbf{k})\mathbf{u}(\mathbf{k}), \tag{3.1}$$

with

$$H(\mathbf{k})=\omega_{\mathrm{TO}}^2 a_0^2 \begin{bmatrix} Ak_x^2+B(k_y^2+k_z^2) & Ck_xk_y & Ck_xk_z \\ Ck_yk_x & Ak_y^2+B(k_z^2+k_x^2) & Ck_yk_z \\ Ck_zk_x & Ck_zk_y & Ak_z^2+B(k_x^2+k_y^2) \end{bmatrix} , \tag{3.2}$$

where A, B, and C are the parameters describing the dispersion in the vicinity of the Γ point. There is a correspondance with Eq. (2.12) in the linear-chain model that $\alpha_1=A$ for longitudinal modes and $\alpha_1=B$ for transverse modes.

The inclusion of long-range Coulomb forces causes a complication because it gives rise to a term singular at zero wave number in the dynamical matrix. This singular term corresponds to a macroscopic electric field due to the polarization $\mathbf{P}(\mathbf{r})$ in the long-wavelength limit. Apart from the singular term, other contributions from the Coulomb forces (including the so-called local-field correction) may be treated in a manner similar to the case of short-range forces expressed in terms of force constants, i.e., they just modify the parameters A, B, C, and ω_{TO}.

The inclusion of the macroscopic electric field introduces two additional terms in the right-hand side of Eq. (3.1) that cannot be expressed in the form of $H(\mathbf{k})$. The most important term is expressed as $\omega_p^2 S\mathbf{u}(\mathbf{k})$ with

$$S=\frac{1}{k^2}\begin{bmatrix} k_x^2 & k_xk_y & k_xk_z \\ k_yk_x & k_y^2 & k_yk_z \\ k_zk_x & k_zk_y & k_z^2 \end{bmatrix} , \tag{3.3}$$

and

$$\omega_p^2=\omega_{\mathrm{LO}}^2-\omega_{\mathrm{TO}}^2=\frac{4\pi nZ^2e^2}{M_r\epsilon_\infty} , \tag{3.4}$$

where n is the density of ion pairs, Ze the effective charge of a cation, and ϵ_∞ the optical dielectric constant. This term gives rise to the frequency splitting of LO and TO phonons at the Γ point, which is the most important result of the long-range Coulomb interaction.

In addition to the splitting of LO and TO phonons, the macroscopic electric field gives rise to a slight modification of the dispersion, i.e., introduces the term $H'\mathbf{u}(\mathbf{k})$ on the right-hand side of Eq. (3.1). We have

$$H'=-\tfrac{1}{2}(\Gamma\omega_{\mathrm{TO}})^2\left[1-\frac{1}{1+\omega_p^2/\omega_{\mathrm{TO}}^2}\right](K^2S+SK^2)a_0^2 , \tag{3.5}$$

with

$$K=\begin{bmatrix} 0 & k_z & k_y \\ k_z & 0 & k_x \\ k_y & k_x & 0 \end{bmatrix} , \tag{3.6}$$

where Γ, corresponding to γ in Eq. (2.9), is the parameter which represents the mixing between acoustic and optical modes, and is expressed by short-range force constants. The corresponding singular term in acoustic branches was discussed in connection with the piezoelectric effect.[31] Of course, H' does not contribute to transverse modes. Further, contributions to longitudinal modes are also not important. As a matter of fact, the valence-force-field model introduced in Sec. III B shows that the inclusion of H' increases the dispersion of longitudinal modes with wave vector in the [111] direction by 10% for InAs, 8% for GaAs, and 4% for GaSb. The increase is somewhat smaller for modes with wave vector in the [110] direction and completely absent for the [001] direction because $KS=SK=0$. In the following we neglect H' since main effects of long-range Coulomb forces have already been taken into account by the term $\omega_p^2 S$.

In the real-space representation, we have

$$(\omega^2-\omega_{\mathrm{TO}}^2)\mathbf{u}(\mathbf{r})=H\left[-i\frac{\partial}{\partial\mathbf{r}}\right]\mathbf{u}(\mathbf{r})-\frac{Ze}{M_r}\mathbf{E}(\mathbf{r}) , \tag{3.7}$$

where the macroscopic electric field $\mathbf{E}(\mathbf{r})$ is

$$\mathbf{E}(\mathbf{r})=\frac{\partial}{\partial\mathbf{r}}\int d\mathbf{r}'\frac{\partial}{\partial\mathbf{r}'}\cdot\mathbf{P}(\mathbf{r}')/\epsilon_\infty|\mathbf{r}-\mathbf{r}'| , \tag{3.8}$$

with the polarization vector $\mathbf{P}=nZe\mathbf{u}$.

It may help us understand the meaning of Eq. (3.7) to consider, for example, a rigid-ion model in which interion forces are described by a finite number of force constants and fixed effective charges of cations and anions. In the long-wavelength limit, optical vibration produces dipoles at each lattice site with the same direction and magnitude. The conventional method to calculate forces acting on an ion due to the dipoles is to consider an imaginary sphere concentric with the reference ion whose radius is much larger than the lattice constant but smaller than the wavelength of phonons. Outside the sphere, the dipoles are safely replaced by a polarization in continuum. Since the macroscopic electric field $\mathbf{E}(\mathbf{r})$ expressed by Eq. (3.8) is due to continuum polarization both outside and inside the sphere, the total local electric field on the ion is written as $\mathbf{E}_{\mathrm{loc}}=\mathbf{E}+\mathbf{E}_{\mathrm{corr}}$, where the so-called local-field correction $\mathbf{E}_{\mathrm{corr}}$ is the contribution from the discrete dipoles inside the sphere subtracted by the field due to homogeneously polarized sphere. As is well known, the sum of fields of discrete dipoles inside a sphere vanishes at a site with cubic symmetry and the sphere polarized uniformly gives rise to the field $-(4\pi/3)\mathbf{P}$, leading to the Lorentz relation $\mathbf{E}_{\mathrm{loc}}=\mathbf{E}+(4\pi/3)\mathbf{P}$. Consequently, the introduction of the effective charges gives rise to the shift of the TO frequency at the Γ point, $\omega_{\mathrm{TO}}^2=\omega_0^2-\omega_p^2/3$, and the LO frequency, $\omega_{\mathrm{LO}}^2=\omega_0^2+2\omega_p^2/3$, where ω_0 is the frequency of TO and LO phonons in the case of vanishing effective charge. In Eq. (3.7), the local-field correction $(4\pi/3)\mathbf{P}$ has been included into ω_{TO}^2 on the left-hand side. The effective charge also modifies the dispersion relation in the rigid-ion model. The major part of such

modification can be taken into account by an appropriate change in parameters such as A, B, and C in Eq. (3.2). There remain some contributions which give rise to the singular correction to the dispersion, i.e., the term H'. These extra contributions are small and not important in usual III-V compound semiconductors.

Using the z-dependent part of the envelope function,

$$\zeta_\nu(x,y,z)=\zeta_\nu(k_x,k_y,z)e^{ik_x x+ik_y y} \quad (\nu=x,y,z) , \tag{3.9}$$

the connection rule can be expressed as

$$\begin{pmatrix} \zeta_{Bx} \\ \nabla\zeta_{Bx} \\ \zeta_{By} \\ \nabla\zeta_{By} \\ \zeta_{Bz} \\ \nabla\zeta_{Bz} \end{pmatrix} = T_{BA} \begin{pmatrix} \zeta_{Ax} \\ \nabla\zeta_{Ax} \\ \zeta_{Ay} \\ \nabla\zeta_{Ay} \\ \zeta_{Az} \\ \nabla\zeta_{Az} \end{pmatrix} , \tag{3.10}$$

with 6×6 interface matrix T_{BA}. Here, ζ is **U** for acoustic modes and **u** for optical modes. Inclusion of the macroscopic electric field does not change T_{BA} because the macroscopic-field term is canceled in subtracting the bulk equation from the equation near the interface as we did in Sec. II B.

In the coordinate system (ξ,η) rather than (x,y), the interface matrix has the following form in the long-wavelength limit:

$$T_{BA}=\begin{pmatrix} T_\xi & 0 & k_\xi a_0 T_1 \\ 0 & T_\eta & k_\eta a_0 T_2 \\ k_\xi a_0 T_3 & k_\eta a_0 T_4 & T_z \end{pmatrix} , \tag{3.11}$$

where T's are 2×2 matrices, and we have retained the terms up to the order of $k_\xi a_0$ and $k_\eta a_0$. We must neglect components t_{12} and t_{22} in T_j $(j=1,\ldots,4)$, which give contributions of the order of $k_\xi a_0 k_z a_0$ or $k_\eta a_0 k_z a_0$. The component t_{21} is the most important in these matrices. Since T_ξ and T_η are, in general, different, the fourfold symmetry with respect to the z axis in the bulk lattice dynamics reduces to the twofold one in the presence of interfaces.

In general cases the k-linear off-diagonal blocks may have some influence on the connection rule. However, there are many cases in which they can be neglected because the wave number k parallel to the interface is sufficiently small. In the discussion of the electron-phonon interaction, for example, it is sufficient to consider the phonon modes with $k\lesssim k_F$ or $k\lesssim k_T$, where k_F is the Fermi wave number and $\hbar^2k_T^2/2m\sim k_B T_e$ with effective mass m, Boltzmann constant k_B, and electron temperature T_e. Usually, $k_F\sim10^{-2}(2\pi/a)$ and $k_T\lesssim10^{-1}(2\pi/a)$, which makes the off-diagonal blocks negligible unless T_j's $(j=1,\ldots,4)$ are exceptionally large. The off-diagonal blocks are neglected hereafter and the connection rule in the linear-chain model $(k_\xi=k_\eta=0)$ is used.

We can show that the off-diagonal blocks are neglected for any values of k_ξ and k_η in the following two cases.

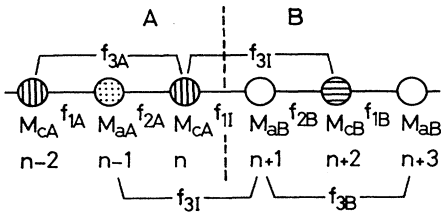

FIG. 4. Linear-chain model for a single heterostructure with second-neighbor force constants f_{3A}, f_{3I}, and f_{3B}.

Case 1: where $|t_{21}|\gg1$ in T_ξ, T_η, and T_z. Since ζ_A and ζ_B are quite small at the interface, the contributions from t_{11} and t_{21} in T_j's $(j=1,\ldots,4)$ are also negligible. Although $|t_{21}|\sim1$ in the connection of optical modes at the InAs/GaSb interface discussed in Sec. IV A, and in that of double heterostructures in Appendix B, these have a qualitative feature of case 1.

Case 2: where the bulk parameters for phonons in A and B are close to each other, and therefore T_j $(j=1,\ldots,4)$ are small. The connection rules for optical modes at GaAs/Ge interfaces and acoustic modes correspond to this case.

B. Valence-force-field model

We adopt the valence-force-field model[32] to find the expression of parameters A, B, C, and ω_{TO} in Eq. (3.2), and take the simplest model in which only the restoring forces against the bond stretching and bond bending are taken into account. The corresponding force constants F_r and F_θ are defined by the energies

$$E_r=\tfrac{1}{2}F_r(\delta r)^2 \quad \text{and} \quad E_\theta=\tfrac{1}{2}F_\theta(r_0\delta\theta)^2 , \tag{3.12}$$

where δr is the deviation of the bond length between ad-

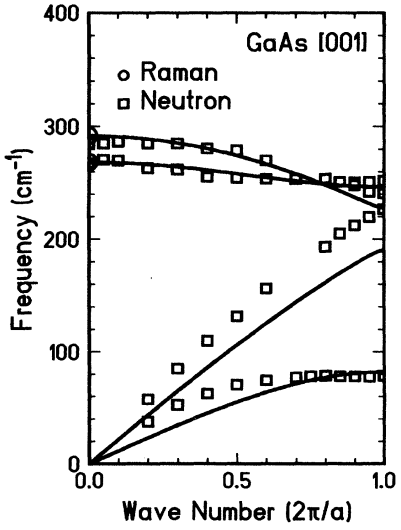

FIG. 5. Dispersion relation of phonons in bulk GaAs in the [001] direction calculated in the present valence-force-field model, together with the experimental results, Raman data (circles), and neutron data (squares) from footnotes d and e in Table I, respectively.

TABLE I. Bulk parameters for five semiconductors. The observed frequencies of LO and TO modes at the Γ and X points are given in units of cm^{-1}, together with the calculated TO frequencies at the X point in the valence-force-field model with use of the observed value of $\omega_{TO}(\Gamma)$ and the ratio of force constants $F_\theta/F_r=0.025$. Also given are the magnitude of the effective charge Ze, the value of optical dielectric constant ϵ_∞, and the mass ratio of cation and anion.

	InAs	GaSb	GaAs	Ge	AlAs
$\omega_{LO}(\Gamma)$ (cm^{-1})	243.3±2[a]	240.3±2[a]	291.9[d]	301[f]	404.1[g]
$\omega_{TO}(\Gamma)$	218.9±3[a]	230.5±3[a]	268.6[d]		360.9[g]
$\omega_{TO}(X)$	218.5[b]	212[c]	252[e]	273[f]	
(calc)	(202)	(213)	(247)	(277)	(336)
$\omega_{LO}(X)$	203[b]	212[c]	241[e]	238[f]	
$Z\epsilon_\infty^{-1/2}$	0.76	0.49	0.66	0.0	0.78
ϵ_∞	12.3	14.4	10.9	15.8	8.16
$r_m=\left[\frac{M_a}{M_c}\right]^{1/2}$	0.808	1.32	1.04	1.0	1.67

[a] $T=4$ K. Infrared reflection. M. Hass and B. W. Henvis, J. Phys. Chem. Solids **23**, 1099 (1962).
[b] $T=100$ K. Second-order Raman scattering. R. Carles, N. Saint-Cricq, J. B. Renucci, M. A. Renucci, and A. Zwick, Phys. Rev. B **22**, 4804 (1980).
[c] $T=300$ K. Neutron scattering. M. K. Farr, J. G. Traylor, and S. K. Sinha, Phys. Rev. B **11**, 1587 (1975).
[d] $T=300$ K. Raman scattering. A. Mooradian and G. B. Wright, Solid State Commun. **4**, 431 (1966).
[e] $T=296$ K. Neutron scattering. G. Dolling and J. L. T. Waugh, in *Lattice Dynamics*, edited by R. F. Wallis (Pergamon, Oxford, 1965), p. 19.
[f] $T=300$ K. Neutron scattering. G Nilsson and G. Nelin, Phys. Rev. B **6**, 3777 (1972).
[g] $T=300$ K. Raman scattering. A. Onton, in *Proceedings of the 10th International Conference on the Physics of Semiconductors, Cambridge, Mass., 1970*, edited by S. P. Keller, J. C. Hensel, and F. Stern (U.S. AEC, Oak Ridge, Tenn., 1970), p. 107.

jacent atoms from the equilibrium value r_0, and $\delta\theta$ is the deviation of the angle between adjacent bonds with one atom in common from the equilibrium. We make a simplification that the value of F_θ does not depend on whether the angle is made up of cation-anion-cation or anion-cation-anion.

The bulk dynamical matrix, the parameters A, B, C, and ω_{TO}^2, and the relation between envelope functions and displacements are given in terms of F_r and F_θ in Appendix E. The corresponding linear-chain model has first- and second-neighbor forces as shown in Fig. 4. Force constants f_1, f_2, and f_3 are related to F_r and F_θ in Appendix E. The second-neighbor forces (f_3) introduce evanescent waves near the interface and the interface matrix is no longer given in an analytical form. The calculation procedure is shown in Appendix F. The force constants at the interface are assumed to be the average of those of the constituent materials, although the calculation is possible for any values.

Three parameters, F_r, F_θ, and the effective charge Ze, are determined as follows. Since we mainly discuss optical modes in the present paper, we use the observed frequencies of LO and TO modes at the Γ point (Table I). The relations between them are given by

$$\omega_{TO}^2=\frac{4}{3M_r}(F_r+8F_\theta)\ , \tag{3.13}$$

and Eq. (3.4). The obtained effective charge Ze is shown in Table I as $Z\epsilon_\infty^{-1/2}$. We should use the curvatures at the Γ point to fix the remaining degree of freedom. Unfortunately, there is no accurate information, except in the case of Ge.[33] Therefore, by taking as a reference the observed frequencies of the TO mode at the X point given in Table I, we determine the ratio F_θ/F_r to be 0.025 for all materials. The calculated TO frequencies at the X point with this ratio are also shown in the table. The resulting dispersion curves, for example, of GaAs are shown in Fig. 5, together with experimental results. In the calculation of the LO branch, the macroscopic electric field is taken into account as in Eq. (3.7). In spite of its simplicity, the present model reproduces the experimental frequencies of optical modes well, except near X, where the calculated frequencies of LO modes deviate downward from the observed ones because of the limitation of the simple valence-force-field model.

IV. APPLICATIONS TO InAs/GaSb AND GaAs/Ge SUPERLATTICES

A. Interface matrices

In this section we discuss optical phonons in InAs/GaSb and GaAs/Ge superlattices. The connection rules can be written in the form of interface matrices because the bulk frequencies at Γ of optical phonons in each material are close to each other, compared with the bandwidth.

The interface matrices for acoustic and optical modes are listed in Tables II and III, respectively. These are calculated with the second-neighbor forces taken into ac-

TABLE II. Interface matrices T_{BA} for acoustic modes. T(GaSb←InAs) represents the interface matrix for the interface atomic configuration InAs/GaSb. Only the diagonal blocks T_ξ, T_η, and T_z are shown.

	B A T(GaSb←InAs)	B A T(GaSb←InAs)
ξ	$\begin{bmatrix} 1.00 & 0.17 \\ 0.00 & 0.92 \end{bmatrix}$	$\begin{bmatrix} 1.00 & 0.17 \\ 0.00 & 0.92 \end{bmatrix}$
η	$\begin{bmatrix} 1.00 & -0.17 \\ 0.00 & 0.92 \end{bmatrix}$	$\begin{bmatrix} 1.00 & -0.18 \\ 0.00 & 0.92 \end{bmatrix}$
z	$\begin{bmatrix} 1.00 & 0.00 \\ 0.00 & 0.92 \end{bmatrix}$	$\begin{bmatrix} 1.00 & 0.00 \\ 0.00 & 0.92 \end{bmatrix}$
	T(Ge←GaAs)	T(Ge←GaAs)
ξ	$\begin{bmatrix} 1.00 & -0.03 \\ 0.00 & 0.79 \end{bmatrix}$	$\begin{bmatrix} 1.00 & 0.00 \\ 0.00 & 0.79 \end{bmatrix}$
η	$\begin{bmatrix} 1.00 & 0.03 \\ 0.00 & 0.79 \end{bmatrix}$	$\begin{bmatrix} 1.00 & -0.01 \\ 0.00 & 0.79 \end{bmatrix}$
z	$\begin{bmatrix} 1.00 & -0.01 \\ 0.00 & 0.79 \end{bmatrix}$	$\begin{bmatrix} 1.00 & -0.01 \\ 0.00 & 0.79 \end{bmatrix}$

TABLE III. Interface matrices T_{BA} for optical modes. T(GaSb←InAs) represents the interface matrix for the interface atomic configuration InAs/GaSb. Only the diagonal blocks T_ξ, T_η, and T_z are shown.

	B A T(GaSb←InAs)	B A T(GaSb←InAs)
ξ	$\begin{bmatrix} 0.99 & 0.15 \\ 0.43 & 1.02 \end{bmatrix}$	$\begin{bmatrix} 1.30 & -0.26 \\ -2.99 & 1.32 \end{bmatrix}$
η	$\begin{bmatrix} 1.38 & 0.26 \\ 3.03 & 1.26 \end{bmatrix}$	$\begin{bmatrix} 0.97 & -0.14 \\ -0.43 & 1.03 \end{bmatrix}$
z	$\begin{bmatrix} 1.07 & 0.28 \\ 1.10 & 1.18 \end{bmatrix}$	$\begin{bmatrix} 1.08 & -0.28 \\ -1.11 & 1.17 \end{bmatrix}$
	T(Ge←GaAs)	T(Ge←GaAs)
ξ	$\begin{bmatrix} 0.83 & -0.01 \\ -0.05 & 0.95 \end{bmatrix}$	$\begin{bmatrix} 0.84 & 0.01 \\ 0.08 & 0.95 \end{bmatrix}$
η	$\begin{bmatrix} 0.83 & -0.01 \\ -0.37 & 0.97 \end{bmatrix}$	$\begin{bmatrix} 0.84 & 0.01 \\ 0.02 & 0.95 \end{bmatrix}$
z	$\begin{bmatrix} 0.78 & -0.02 \\ -0.13 & 1.02 \end{bmatrix}$	$\begin{bmatrix} 0.77 & 0.02 \\ 0.02 & 1.02 \end{bmatrix}$

count. Neglect of the second-neighbor forces gives, at most, 10% deviation, however. Two atomic configurations, InAs/GaSb and InAs/GaSb, are possible at the interface of InAs in A ($z<0$) and GaSb in B ($z>0$). The latter corresponds to the case that the interface consists of As and Ga, and the former to the case that the interface consists of In and Sb. The same is applicable to GaAs/Ge interfaces.

In the case of optical modes, the sign of t_{21} is different between the two configurations at InAs/GaSb interfaces: $t_{21}>0$ for InAs/GaSb and $t_{21}<0$ for InAs/GaSb. Since the reduced mass of the ion pair In-Sb (As-Ga) at the interface is larger (smaller) than those in the constituent semiconductors, the frequency of the corresponding vibration mode is lower (higher). This gives a repulsive (attractive) δ-function potential at the interface that corresponds to a positive (negative) value of t_{21}, as has been discussed in Sec. II B. Correspondingly, the magnitude of the envelope function is reduced (enchanced) at the interface, as will be shown in Figs. 6(b) and 8(b). In particular, localized modes appear at the interfaces when $t_{21}<0$. A similar result is obtained in Appendix B for double heterostructures.

There are large differences between interface matrices T_ξ and T_η for displacements along the ξ [1$\bar{1}$0] and η [110] axes, particularly in the off-diagonal element t_{21} in the case of InAs/GaSb interfaces. The interplanar force constant for transverse modes (ξ and η) takes two values, different by an order of magnitude, depending on the direction of the displacement relative to that of chemical bonds. It takes the larger and smaller values alternatingly along the z axis for each of the ξ and η modes. The force constant at InAs/GaSb interface, for example, is larger for η modes than for ξ, giving rise to a larger value of t_{21} (see Table III). The situation is opposite at the GaSb/InAs interface between GaSb ($z<0$) and InAs ($z>0$). The interface matrix for GaSb/InAs, which is not shown in Table III, is obtained from that for InAs/GaSb (Table III) by the simple transformation given in Appendix D. Note that the interface matrix T_ξ(InAs←GaSb) is related to T_η(GaSb←InAs).

Tables II and III contain interface matrices of GaAs/Ge heterostructures. Since Ga, As, and Ge have almost the same mass, interface matrices for optical modes are nearly the unit matrix, except $t_{21}=-0.37$ for η modes at GaAs/Ge interface. This deviation is presumably due to a large difference in force constants between heteropolar GaAs and homopolar Ge.

B. Numerical procedure

The differential equation for $\mathbf{u}_l$ ($l=A$ or B) at a fixed wave vector $\mathbf{q}=(k_\xi,k_\eta)$ is

$$(\omega^2-\omega_{\mathrm{TO}l}^2)\mathbf{u}_l(\mathbf{q},z)=H_l\left[\mathbf{q},\,-i\frac{\partial}{\partial z}\right]\mathbf{u}_l(\mathbf{q},z)-\frac{Z_l e}{M_{rl}}\mathbf{E}(\mathbf{q},z)\ . \tag{4.1}$$

The macroscopic electric field is given by[23–25]

$$\epsilon_\infty E_i(\mathbf{q},z)=-4\pi\delta_{iz}P_z(\mathbf{q},z)-\frac{2\pi}{q}\int dz' e^{-q|z-z'|}\sum_j K_i K_j P_j(\mathbf{q},z')\quad (i,j=x,y,z)\ , \tag{4.2}$$

with $K=(\mathbf{q}, \mathrm{sgn}(z-z')iq)$, where $\mathrm{sgn}(z)=1$ for $z>0$, and $\mathrm{sgn}(z)=-1$ for $z<0$. The optical dielectric constant ϵ_∞ is assumed to be constant throughout the system because ϵ_∞ does not change so much from material to material, as shown in Table I.

The differential equation is supplemented by the connection rule, which is expressed in the form of energy:

$$E_c=-f_c\sum_i|\tilde{u}_B(z_i)-T_{BAi}\tilde{u}_A(z_i)|^2\ , \tag{4.3}$$

where $\tilde{u}=(u_x,\nabla u_x,u_y,\nabla u_y,u_z,\nabla u_z)^t$ and subscript i distinguishes interfaces. We calculate eigenvalues and eigenvectors of Eqs. (4.1) and (4.3) for a sufficiently large f_c.

One way to solve this eigenvalue problem is to expand the envelope function in terms of an appropriate orthonormal set,

$$(M_{rl})^{1/2}u_{il}(\mathbf{q},z)=\sum_n c_{iln}(\mathbf{q})\psi_{ln}(z)\ , \tag{4.4}$$

where c_{iln}'s are expansion coefficients and ψ_{ln}'s are basis functions. To describe all kinds of connection rules, we consider the following functions:

$$f_{lG}(z)=\begin{cases} f_G(z) & \text{when } z \text{ is in } l \text{ layers}\ , \\ 0 & \text{otherwise}\ , \end{cases} \tag{4.5}$$

with

$$f_G(z)=(N_z d)^{-1/2}e^{i(q_z+G)z}\ , \tag{4.6}$$

where d is the period of superlattice, N_z the number of periods, $-\pi/d<q_z<\pi/d$, and $G=2\pi n/d$ (n an integer). The functions $f_{lG}(z)$ are neither orthogonal to each other nor normalized. An orthonormal set is obtained as

$$\psi_{ln}(z)=\sum_G \sigma_n^{-1/2}b_{nG}f_{lG}(z)\ , \tag{4.7}$$

by using the eigenvalues σ_n and the eigenvectors b_n of the overlap integrals $S^l_{G'G}=\langle lG'|lG\rangle$. We must exclude the functions with quite small σ_n, say less than 10^{-4}.

C. InAs/GaSb

We consider InAs/GaSb superlattices with 10.5 layers of InAs and GaSb in one period, corresponding to $d=64$ Å. In Fig. 6(a) we present dispersion curves for optical phonons in the superlattice with *In*As/Ga*Sb* and Ga*Sb*/*In*As interfaces. Dispersion curves are given along the q_z and k_η axes for values of k_η less than $1/14a_0$, for which the off-diagonal blocks of the interface matrix [T_1, T_2, T_3, and T_4 of Eq. (3.11)] may be neglected. We also show the dependence of frequencies on the direction of wave vector from the z axis ($\theta=0°$) to the η axis ($\theta=90°$) in the vicinity of the Γ point. No ξ modes are shown in the figure because ξ modes are transverse and decoupled from the others. The dispersion curves of ξ modes are the same as those of η modes along the q_z axis, while they are flat when θ is changed. In Fig. 6(b) the envelope multiplied by the square root of the reduced mass is shown for several modes.

LO modes a and b in the left-hand panel of Fig. 6(a) have frequencies above the LO top of GaSb and are confined in InAs "quantum wells" [Fig. 6(b)]. These features have been already shown by Fasolino, Molinari, and Maan.[15] The central panel shows that the frequencies of modes *a-d* and *c-e* have a considerable θ dependence. The mode b is antisymmetric with respect to the center of both layers and has no θ dependence.

For comparison, we show the results of the dielectric continuum model by dotted lines in the same figure. In

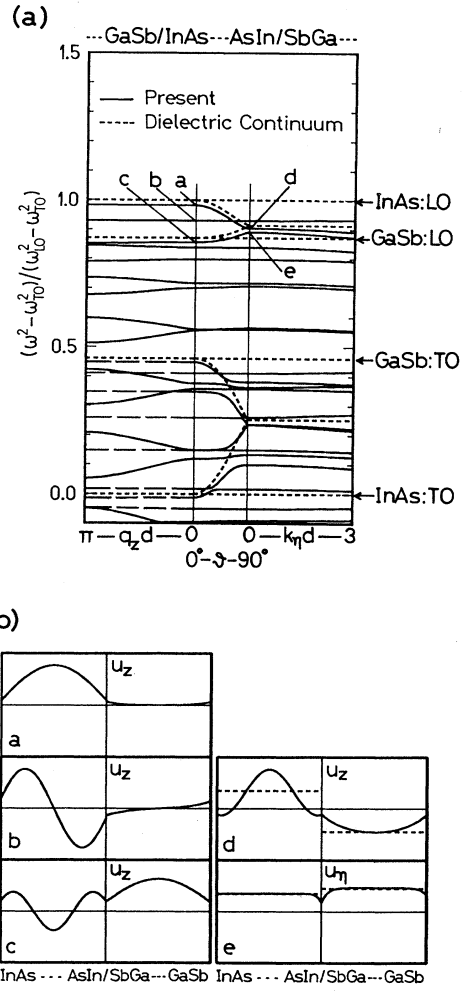

FIG. 6. Optical phonons in an InAs/GaSb superlattice with *In*As/Ga*Sb* and Ga*Sb*/*In*As interfaces. Each layer of superlattice (period $d=64$ Å) has 10.5 layers of InAs or GaSb. (a) Dispersion curves together with those of the dielectric continuum model (dotted lines). Plotted are the squared frequencies ω^2 measured from ω_{TO}^2 of InAs and normalized by $\omega_p^2=\omega_{LO}^2-\omega_{TO}^2$ of InAs. In the central panel the frequencies at the zone center are plotted as a function of θ, the direction of the wave vector. In the left-hand panel longitudinal (solid lines) and transverse modes (dashed lines) are decoupled from each other. (b) Envelope function multiplied by the square root of the reduced mass. Dotted lines in panels *d* and *e* represent the envelopes in the dielectric continuum model of the Fuchs-Kliewer modes at $\theta=90°$ with frequency just above mode *d*.

this model almost all modes are degenerate at the bulk LO and TO frequencies at the Γ point of InAs and GaSb. These degeneracies are resolved by the inclusion of dispersion in the present formalism. There are four modes with considerable θ dependence in the dielectric continuum model, which are called Fuchs-Kliewer modes because they are essentially the same as the modes in the dielectric slab studied by Fuchs and Kliewer.[23] The θ dependence is due to the change of the macroscopic electric field. The corresponding modes in our calculation (*a-d* and *c-e*), which are also called Fuchs-Kliewer modes hereafter, have slightly lower frequencies due to the effect of connection rules and dispersion.

The envelope function of mode *e* with displacement along the η direction is almost the same as the corresponding one in the dielectric continuum model, except that it is modified by the connection rule near the interfaces, i.e., exhibits a downward cusp. The behavior of the envelope function is different at two interfaces within one period of superlattice because the force constants at those interfaces are different for η modes. The thickness of the modified region, which is only about the lattice constant, is determined by the deviation of its frequency from the bulk TO tops of InAs and GaSb and by the width of the TO bands. In fact, as the layer thickness increases, only the flat region increases, as shown in Fig. 7. It is therefore concluded that if the layer thickness is much larger than the lattice constant, the dielectric continuum model describes mode *e* accurately. On the other hand, mode *d*, with displacement along the *z* axis, is strongly modified by the connection rule, even for large layer thickness because its frequency is quite close to the bulk LO tops.

Figure 8 shows the results for the InAs/GaSb superlattice with In*As*/*Ga*Sb and *Ga*Sb/In*As* interfaces. The interfaces consist of Ga and As atomic planes. Three localized modes at the interfaces appear above the LO top of InAs (modes *p*, *q*, and *r* at $\theta=0°$). The highest one (mode *p*) has displacement along the η axis and is localized within Ga and As atomic planes at one of the two interfaces at which the force constant is larger. The localized mode with displacement along ξ, which is not shown in Fig. 8, has amplitude at the other interface at which the force constant for ξ modes is larger. On the other hand, the localized *z* modes (modes *q* and *r*) have amplitude at both interfaces and are extended over several atomic planes. The frequency is 1.272 for mode *p* and 1.206 for mode *q* in the same units as in the figure, whereas the value is 0.937 and 1.196, respectively, when calculated by the standard lattice dynamics with the same valence-

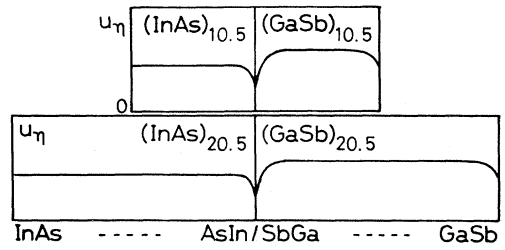

FIG. 7. Period dependence of the envelope of a Fuchs-Kliewer mode at $\theta=90°$ (mode *e* in Fig. 6). The envelope function multiplied by the square root of the reduced mass is plotted.

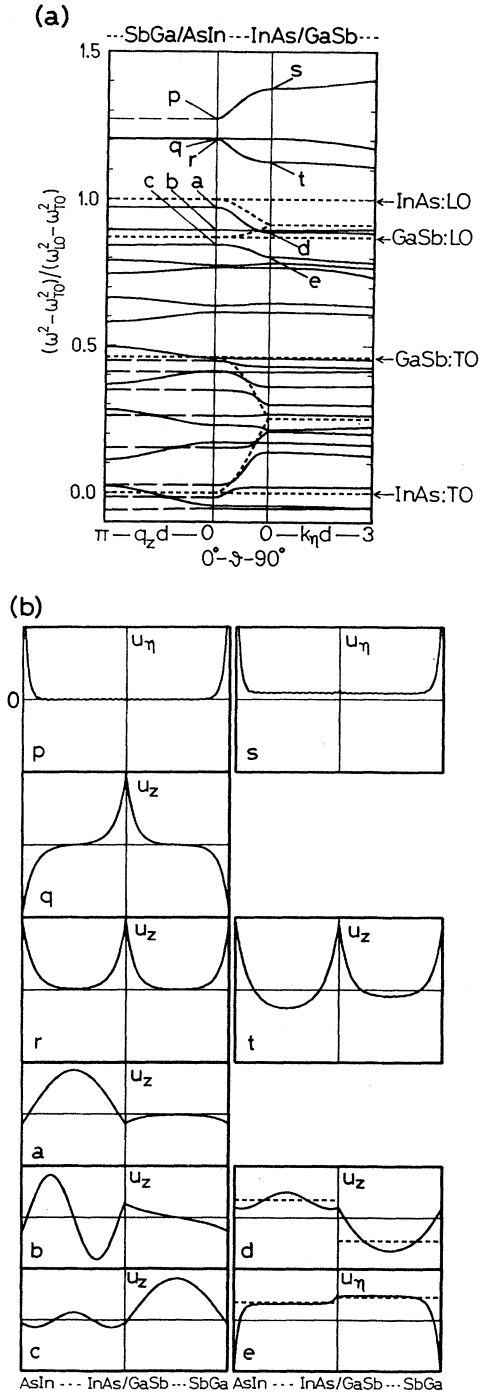

FIG. 8. Optical phonons in an InAs/GaSb superlattice with In*As*/*Ga*Sb and *Ga*Sb/In*As* interfaces. Each layer of superlattice (period $d=64$ Å) has 10.5 layers of InAs or GaSb. (a) Dispersion curves. (b) Envelope function multiplied by the square root of the reduced mass. See the caption of Fig. 6 for more explanations.

force-field parameters and effective charges. The long-wavelength approximation has started to break down for TO mode p because the deviation of its frequency from the tops of bulk TO bands is comparable to their bandwidths, whereas it applies well to LO mode q.

As shown in Fig. 8(a), the interface modes exhibit a strong θ dependence of frequency, which is due to the macroscopic electric field just as in the case of the Fuchs-Kliewer modes. The θ dependence of frequency of mode c-e (one of the Fuchs-Kliewer modes) is quite different from that calculated in the dielectric continuum model, which is understood by the strong level repulsion between modes with η displacements, c-e and p-s. The envelope function of mode e [Fig. 8(b)] has a sharp peak at one of two interfaces due to the mixing of the interface mode (mode p). The interface modes at $\theta=90°$ (panel s and t) have displacement inside layers, which is induced by the macroscopic electric field.

The interface modes were first found by Fasolino, Molinari, and Maan using a linear-chain model for transverse modes (ξ and η modes[13]) and for longitudinal modes.[14] The frequencies and displacement patterns in our calculation are in good agreement with those in their calculation, except the frequency position of transverse modes (mode p). As shown in their calculation, there are also interface modes in the InAs/GaSb superlattice with In-Sb interfaces, which have frequencies below the optical bands of InAs and GaSb. The present formalism treating long-wavelength phonons is not applicable to these interface modes.

A recent paper[15] of Fasolino, Molinari, and Maan showed the presence of resonant LO modes, which exhibit a quasiconfined behavior in spite of their frequency positions in the overlapping region of bulk LO bands. In our calculation, mode c in Fig. 6(b) (InSb interface) and in Fig. 8(b) (GaAs interface) show a resonant behavior. In the case of InSb interfaces, such behavior is understood by the presence of a repulsive δ-function potential at two interfaces (Sec. IV A), just like the behavior of the electron wave function in double-barrier structures. On the other hand, the potential at GaAs interfaces is attractive, but the amplitude of mode c is small at the interfaces in order to be orthogonal to the interface modes (modes q and r), leading to a well-defined resonant mode.

D. GaAs/Ge

Figure 9 presents the results for the GaAs/Ge superlattice with *Ga*As/*Ge* and *Ge*/*Ga*As interfaces. Each period, $d=59$ Å, contains 10.5 layers of GaAs and 21 layers of Ge, i.e., the GaAs and Ge layers have the same thickness. The main difference with InAs/GaSb systems is that Ge is homopolar, leading to no Fuchs-Kliewer modes originating from Ge. The left-hand panel shows the features similar to those of InAs/GaSb superlattices, i.e., the existence of confined and extended modes due to the difference of bulk frequencies. Since the interface matrix is close to the unit matrix, the magnitude of gaps appearing at the zone center and boundary is smaller than that of InAs/GaSb superlattices and the envelope functions connect almost continuously at the interfaces.

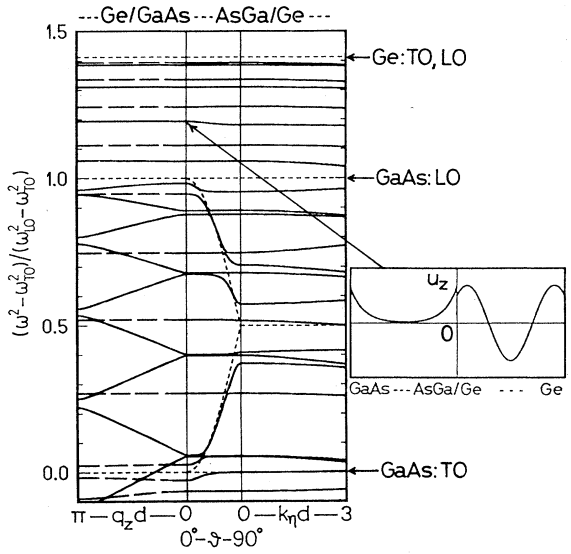

FIG. 9. Dispersion curves for optical phonons in a GaAs/Ge superlattice with *Ga*As/*Ge* and *Ge*/*Ga*As interfaces. Each layer of superlattice (period $d=59$ Å) has 10.5 layers of GaAs or 21 layers of Ge. Plotted are the squared frequencies ω^2 measured from ω_{TO}^2 of GaAs and normalized by $\omega_p^2=\omega_{LO}^2-\omega_{TO}^2$ of GaAs. The right-hand panel presents the envelope function multiplied by the square root of the reduced mass for the mode marked by arrow. See the caption of Fig. 6 for details.

V. GaAs/AlAs HETEROSTRUCTURES

In the GaAs/AlAs systems, where the bulk optical bands have a large gap between them, all optical phonons are nearly confined in one of the layers. Because of the large frequency separation, we can safely replace the AlAs layer by a dielectric continuum when discussing phonons in the GaAs layer, and vice versa. For modes in the vicinity of the zone-center frequency of bulk GaAs, displacements in the GaAs layer are described by envelopes which satisfy the integro-differential equation (3.7) and should be connected to actual displacements of Al and As ions in the AlAs layer. This leads to a kind of boundary conditions for the envelopes. The same is certainly applicable to modes in the vicinity of the frequency of bulk AlAs. In the following, we shall show that the boundary conditions are approximately such that the envelopes should vanish at a boundary plane and determine its position, starting with lattice dynamics.

First, we consider phonon modes mainly confined in the GaAs layer. We use the linear-chain model with only first-neighbor forces shown in Fig. 3. Consider an interface of $A=$GaAs ($z<0$) and $B=$AlAs ($z>0$) and choose the zero of the z axis at the middle point between the interfacial As and Al atomic planes. The force constants in the GaAs and AlAs layers including the interface region are assumed to be the same because the valence-force-field parameters F_r and F_θ coincide in two materials within 2%.[18] From the equations of motion for the interfacial As and Al ions, we obtain a relation similar to that given in Eq. (2.18):

$$u_{aA}(n+1)=u_{aB}(n+1) \quad \text{at } z=-a_0/2\ ,$$
$$u_{cA}(n+2)=u_{cB}(n+2) \quad \text{at } z=a_0/2\ . \tag{5.1}$$

In case of longitudinal modes, the displacements in the GaAs layer are

$$u_{aA}(n+1)=-\frac{M_{\mathrm{Ga}}}{M_{\mathrm{Ga}}+M_{\mathrm{As}}}u\left[-\frac{a_0}{2}\right]\ ,$$
$$u_{cA}(n+2)=\frac{M_{\mathrm{As}}}{M_{\mathrm{Ga}}+M_{\mathrm{As}}}u\left[\frac{a_0}{2}\right]\ , \tag{5.2}$$

using the envelope function u. On the other hand, the displacements in the AlAs layer are given by a linear combination of an evanescent gap mode χ and a mode ψ induced by a macroscopic electric field:

$$u_{aB}(n+1)=\chi_{\mathrm{As}}+\psi_{\mathrm{As}} \quad \text{and} \quad u_{cB}(n+2)=\chi_{\mathrm{Al}}+\psi_{\mathrm{Al}}\ , \tag{5.3}$$

where $\psi_{\mathrm{Al}}/\psi_{\mathrm{As}}=-(M_{\mathrm{As}}/M_{\mathrm{Al}})(E_{\mathrm{Al}}/E_{\mathrm{As}})$, with macroscopic electric field E_{Al} and E_{As} at Al and As planes, respectively. Using the above equations and the Taylor expansion $u(\epsilon a_0)=u(0)+\epsilon\nabla u$, we have

$$u(z_0)=f_\psi\ ,$$

with

$$f_\psi=\frac{1+M_{\mathrm{Ga}}/M_{\mathrm{As}}}{\alpha+M_{\mathrm{Ga}}/M_{\mathrm{As}}}(\alpha\psi_{\mathrm{Al}}-\psi_{\mathrm{As}})\ ,$$
$$z_0=\frac{\alpha-M_{\mathrm{Ga}}/M_{\mathrm{As}}}{\alpha+M_{\mathrm{Ga}}/M_{\mathrm{As}}}(a_0/2)\ , \tag{5.4}$$

where $\alpha=\chi_{\mathrm{As}}/\chi_{\mathrm{Al}}$ at the TO frequency of bulk GaAs is shown to be 0.77 by the lattice dynamics in bulk AlAs. Usually, the displacement in the AlAs layer, ψ, due to a macroscopic electric field is quite small compared to that in the GaAs layer. Therefore, Eqs. (5.4) lead to the boundary condition that the envelope should vanish at $z_0=-0.05a_0$, i.e., close to the midpoint between the interfacial As and Al planes. In a hypothetical case in which α is infinite, i.e., in the case of infinite frequency separation, the node of the envelope is just at the Al plane, as was pointed out by Jusserand and Paquet.[34]

Similarly, the boundary conditions for transverse modes are given by $u(z_0)=0$ with

$$z_0=\left[0.5\frac{\alpha-M_{\mathrm{Ga}}/M_{\mathrm{As}}}{\alpha+M_{\mathrm{Ga}}/M_{\mathrm{As}}}+\frac{(\alpha-1)(2F-1)}{(1+M_{\mathrm{As}}/M_{\mathrm{Ga}})(\alpha+M_{\mathrm{Ga}}/M_{\mathrm{As}})}\right]a_0\ , \tag{5.5}$$

where F is defined in Eq. (2.4). Explicitly, we have $\alpha=0.28$ and $F=0.125$ for ξ modes and $\alpha=7.4$ and $F=0.875$ for η modes, which give $z_0^\xi=-0.05a_0$ and $z_0^\eta=0.67a_0$. The difference in "boundary" position for ξ and η modes leads to mixings of x and y displacements at the interface. The boundary conditions written in terms of x and y displacements are

$$u_x(z_{\mathrm{av}})+\delta z\frac{\partial u_y}{\partial z}=0 \quad \text{and} \quad u_y(z_{\mathrm{av}})+\delta z\frac{\partial u_x}{\partial z}=0\ , \tag{5.6}$$

with $z_{\mathrm{av}}=(z_0^\xi+z_0^\eta)/2$ and $\delta z=(z_0^\xi-z_0^\eta)/2$. Such mixings are negligible when the wavelength is much larger than δz.

There are a few cases in which the field-induced displacement ψ may not be negligible. Typical examples are the Fuchs-Kliewer modes at $\theta=90°$, for which the macroscopic electric field in the AlAs layer is large. For such modes, the electric field and, consequently, the amplitude of displacements in the AlAs layer are estimated to good accuracy by using the dielectric continuum model. In the dielectric continuum model the envelopes of displacements are constant in each of the A and B layers, and the ratio of them is given by

$$\frac{u_B}{u_A}=\frac{Z_BE_BM_{rA}(\omega^2-\omega_{\mathrm{TO}A}^2)}{Z_AE_AM_{rB}(\omega^2-\omega_{\mathrm{TO}B}^2)}\ , \tag{5.7}$$

where $A=$GaAs and $B=$AlAs. Here, $E_B=-E_A$ for the Fuchs-Kliewer mode at $\theta=90°$ with z displacement, whereas $E_B=E_A$ for those with ξ and η displacement. By estimating ψ by the above equation, we obtain f_ψ in Eq. (5.4) to be $f_\psi/u_A=0.06$, -0.13, and -0.23 for the Fuchs-Kliewer modes with z, ξ, and η displacements, respectively, which is small, but certainly not negligible. Fortunately, however, this does not cause serious problems because these modes are mainly determined by the macroscopic electric field and are insensitive to the boundary conditions. Therefore, we conclude that the above boundary conditions are also applicable when the wave vector is not perpendicular to the interface. This conclusion does not depend on the model of force constants.

Similar boundary conditions can be obtained for AlAs-like modes, i.e., for modes whose frequency is close to that of optical phonons of AlAs. We consider an interface of AlAs ($z<0$) and GaAs ($z>0$), and choose the zero of the z axis at the midpoint of the interfacial As and Ga atomic planes. Then, the boundary conditions read that the envelopes should vanish at $z_0=0.58a_0$, $0.34a_0$, and $0.74a_0$ for z, ξ, and η modes, respectively. Here, we have used the values of $\chi_{\mathrm{As}}/\chi_{\mathrm{Ga}}$, -4.8, -2.8, and -18 for z, ξ, and η modes, respectively, at the TO frequency of bulk AlAs. Contributions of field-induced displacements ψ in Eq. (5.4) are $f_\psi/u_A=-0.12$, 0.07, and 0.09 for the AlAs-like Fuchs-Kliewer modes at $\theta=90°$ with z, ξ, and η displacements, respectively, where u_A is the envelope in the AlAs layer estimated using the dielectric continuum model.

When the present results are applied to a $(\mathrm{GaAs})_n(\mathrm{AlAs})_m$ superlattice, the effective thickness in the case of GaAs-like optical phonons is $d(\mathrm{GaAs,LO})=(n+0.5)a/2$ for longitudinal and $d(\mathrm{GaAs,TO})=(n+0.8)a/2$ for transverse modes. In the case of AlAs-like phonons, on the other hand, it is $d(\mathrm{AlAs,LO})=(m+1.1)a/2$ for longitudinal and $d(\mathrm{AlAs,TO})=(m+1.0)a/2$ for transverse modes. These values are in good agreement with the results previously obtained in a rigid-ion valence-force-field model.[18]

Many works have been devoted to determining the effective thickness both theoretically[16,17,34–37] and experimentally[38–42] when the wave vector is perpendicular to interfaces ($\theta=0°$). There remain slight discrepancies among theoretical values, which may be largely due to differences in models for force constants. For example, Richter and Strauch[16] obtained the effective thickness $d(\text{GaAs})=(n+1)a/2$ and $d(\text{AlAs})=(m+1)a/2$ for both LO and TO modes. On the other hand, Ren, Chu, and Chang[17] obtained $d(\text{GaAs})=(n+0.5)a/2$ and $d(\text{AlAs})=(m+0.5)a/2$. Our result is closer to that of Richter and Strauch for d(GaAs,TO) and d(AlAs), whereas ours coincides with that of Ren *et al.* for d(GaAs,LO). Ren *et al.* also obtained a similar value of the effective thickness for $\theta=90°$. We have shown here that the same effective thickness is approximately valid for any value of θ.

It is quite easy to make explicit calculations of phonon modes in $(\text{GaAs})_n(\text{AlAs})_m$ superlattices using the present formalism. Examples for long-wavelength GaAs-like modes in a superlattice with $n=m=7$ have been already reported elsewhere.[18] The "boundary" position has been taken to be at the midpoint between the interfacial As and Al planes for all of the ξ, η, and z modes. The results have turned out to be almost identical to those of calculations made in the rigid-ion valence-force-field model,[18] demonstrating its usefulness.

VI. SUMMARY AND CONCLUSIONS

The envelope-function formalism has been constructed for long-wavelength phonons in semiconductor heterostructures. It consists of a set of differential equations for envelope functions of atomic displacements and their boundary conditions at interfaces. Our starting point is the bulk dynamical matrix, and the procedure to derive the formalism is quite similar to that for the effective-mass theory in the electron problem. For acoustic modes our formalism becomes equivalent with the theory of elasticity.

The present formalism is applicable to optical modes in the following two cases: the case that the band-offset is much smaller than the bandwidth, and the case that it is sufficiently larger than the bandwidth. In the former case, the connection rule of envelope functions on both sides of the interface has been obtained in the form of the interface matrix. In several important examples the interface matrices are diagonal with respect to three components $\xi(=x-y)$, $\eta(=x+y)$, and z, and they are independent of k_ξ and k_η, the wave-vector components along the interface. We have obtained various types of connection rules, depending not only on the constituent materials, but also on the microscopic structure of the interface.

As examples, dispersion curves and envelope functions have been calculated for optical phonons in InAs/GaSb and GaAs/Ge superlattices. We have found that in InAs/GaSb superlattices the envelope function exhibits a cusp at the interface, and the type of cusp depends on whether the atomic configuration is In-Sb or As-Ga at the interface. On the other hand, in the GaAs/Ge superlattice the envelope functions connect almost continuously at the interfaces. This variety of the behaviors of phonon modes in the vicinity of the interfaces is mainly determined by a single parameter, t_{21}, the off-diagonal element of the interface matrix: $t_{21}>0$ for the In-Sb interface of InAs/GaSb superlattices, $t_{21}<0$ for the As-Ga interface, and $t_{21}\sim 0$ for the interfaces of GaAs/Ge superlattices. The calculated results have been compared with those obtained using the dielectric continuum model. Several important differences have been found; in particular, our formalism can describe the differences between the two interface configurations and the existence of localized modes at the As-Ga interface of InAs/GaSb superlattices in a unified way.

In GaAs/AlAs heterostructures, where the bulk optical bands of the two materials have a large gap between them, it has been shown that the boundary condition that the envelopes should vanish at interfaces is applicable even when the wave vector is not perpendicular to interfaces.

The most important application of our formalism is the Frölich-type electron-phonon interaction. Several authors discussed the problem using the dielectric continuum model. Lassnig calculated the form factors for the Fröhlich interaction in double heterostructures.[43] Degani and Hipolito calculated the polaron-mass correction in several heterostructures.[44] Wendler and Pechstedt calculated the dispersion curves of plasmon-phonon coupled modes in double heterostructures,[45] which can be observed by use of Raman-scattering and attenuated-total-reflection techniques.[46] The intensity of resonant Raman scattering is also determined by the Fröhlich interaction, and was discussed for simple, confined LO phonons.[39] Our formalism provides a refined basis with which to investigate these properties.

ACKNOWLEDGMENTS

This work has been supported in part by a Grant-in-Aid for Specially Promoted Research from the Ministry of Education, Science and Culture of Japan.

APPENDIX A: MODES NEAR THE ZONE BOUNDARY

We derive the envelop-function formalism for modes near the Brillouin-zone boundary (X point, $k_b=2\pi/a$) using the linear-chain model of Fig. 3. For simplicity, we consider only longitudinal modes ($f_1=f_2$) and neglect the differences among the force constants f_{1A}, f_{1B}, and f_{1I}. The situation is quite analogous to the s-p tight-binding model for electrons considered in Ref. 3. One mode at the X point, in which only cations vibrate, corresponds to the cation s orbital, and the other mode corresponds to the anion p orbital. For wave vectors $k_1a_0\ll 1$ ($k_1=k-k_b$) the $k\cdot p$ Hamiltonian has the same form as that for the s-p tight-binding model around the Γ point:

$$\frac{\omega_{\text{TO}}^2}{r_m+r_m^{-1}}\begin{bmatrix} r_m & k_1a_0 \\ k_1a_0 & r_m^{-1}\end{bmatrix}. \tag{A1}$$

The diagonalized dynamical matrix is

$$\frac{\omega_{\mathrm{TO}}^2}{r_m+r_m^{-1}}\begin{bmatrix} r_m+\dfrac{1}{r_m-r_m^{-1}}(k_1a_0)^2 & 0 \\ 0 & r_m^{-1}-\dfrac{1}{r_m-r_m^{-1}}(k_1a_0)^2 \end{bmatrix}. \tag{A2}$$

The corresponding envelope functions ζ_c and ζ_a are defined by

$$\begin{bmatrix} u_c(k_1+k_b) \\ u_a(k_1+k_b) \end{bmatrix} = \begin{bmatrix} 1 & -hk_1a_0 \\ gk_1a_0 & 1 \end{bmatrix} \begin{bmatrix} \zeta_c(k_1) \\ \zeta_a(k_1) \end{bmatrix}, \tag{A3}$$

where u_c and u_a are the displacements of cation and anion, respectively, $g=1/(r_m^2-1)$, and $h=1/(1-r_m^{-2})$. Hereafter the modes corresponding to ζ_c and ζ_a are called cation and anion modes, respectively.

The interface matrices are as follows. When cation modes are connected,

$$T_{BA}=\begin{bmatrix} 1 & \frac{1}{2}(g_A/g_B-1) \\ 0 & g_A/g_B \end{bmatrix}, \tag{A4}$$

corresponding to the connection of the conduction bands of GaAs and AlAs. This is essentially the same connection as proposed by Babiker for LO modes near the Γ point.[27] When a cation mode in A and an anion mode in B are connected,

$$T_{BA}=\begin{bmatrix} -1/2h_B & 1/4h_B+g_A \\ 1/h_B & -1/2h_B \end{bmatrix}, \tag{A5}$$

corresponding to the connection between the conduction band of InAs and the valence band of GaSb. When $r_{mA}=1$ ($r_{mB}=1$), the determinant of T_{BA} becomes infinity (zero) due to the vanishing of the X-point extremum.

APPENDIX B: INTERFACE MATRICES FOR DOUBLE HETEROSTRUCTURES

Consider the double heterostructure shown in Fig. 10, with a sandwiched layer (I) consisting of a single cation atomic plane. We investigate the connection rule between long-wavelength LO modes in A and B layers. Here we restrict ourselves to the case that A and B are occupied by the same semiconductor. An example is GaAs crystal, in which one Ga atomic plane is replaced by an Al or In plane. Although there is considerable lattice mismatch between A (B) and I in the case of I=In, the structure can be free from defects because the I layer consists of only one atomic plane. Using the relation between the displacements in A and B,

$$\begin{bmatrix} u_{cB}(n) \\ u_{aB}(n+1) \end{bmatrix} = \begin{bmatrix} 1 & 0 \\ 2-M_{cI}\omega_{\mathrm{LO}}^2 f^{-1} & -1 \end{bmatrix} \times \begin{bmatrix} u_{cA}(n) \\ u_{aA}(n-1) \end{bmatrix}, \tag{B1}$$

the interface matrix is

$$t_{11}=t_{22}=1,\quad t_{12}=0,\quad t_{21}=2(1+r_m^2)\left(\frac{M_{cI}}{M_{cA}}-1\right). \tag{B2}$$

In the case of $A=B=$GaAs, $t_{21}=-2.54$ for $I=$Al and $t_{21}=2.69$ for $I=$In. Figure 11 shows the modes with the longest wavelength in superlattices $(GaAs)_9(AlAs)_1$ and $(GaAs)_9(InAs)_1$, which exhibit two types of cusps at the interface, respectively. A localized interface mode appears in the $(GaAs)_9(AlAs)_1$ superlattice, although it is not shown in the figure.

Similarly, the interface matrix for the heterostructure with an anion sandwiched layer is $t_{21}=2(1+r_m^{-2})(M_{aI}/M_{aA}-1)$, with the other elements unchanged.

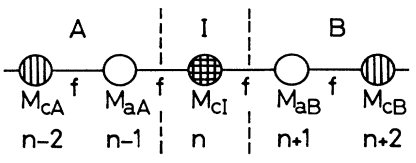

FIG. 10. Linear-chain model for a double heterostructure with a single force constant f. The masses of the cation and anion are denoted by M_c and M_a, respectively.

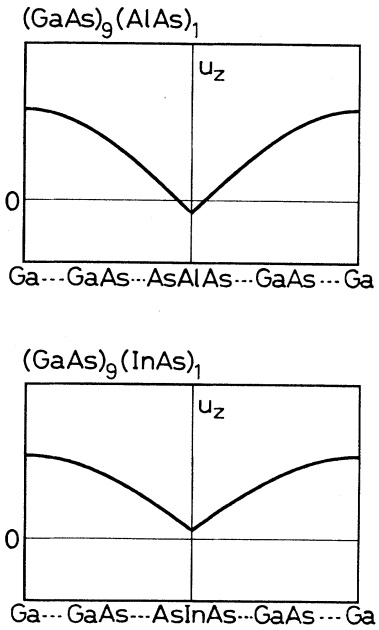

FIG. 11. Envelopes of long-wavelength LO modes in superlattices $(GaAs)_9(AlAs)_1$ and $(GaAs)_9(InAs)_1$.

APPENDIX C: ENERGY-CONSERVATION LAW

The divergence of energy flux must be zero throughout the system in the stationary state. In the case of the linear-chain model (Fig. 3), we have at the interface

$$P_A = P_B \ , \tag{C1}$$

for the z components of the flux. The energy flux is written as

$$P = En\omega \frac{1}{2i} \left[\zeta^* \frac{\partial}{\partial z} \zeta - \zeta \frac{\partial}{\partial z} \zeta^* \right] , \tag{C2}$$

where ζ^* is the complex conjugate of ζ, and n is the density of ion pairs. The coefficient E is

$$E = (M_c + M_a)v^2 \quad \text{and} \quad -M_r v^2 \ , \tag{C3}$$

for acoustic and optical modes around the Γ point, respectively, with the sound velocity v. Equation (C1) leads to the conditions for the interface matrix.[3] First, the interface matrix can be chosen as real, except for an unimportant common phase factor. Second, its determinant is

$$\det(T_{BA}) = E_A / E_B \ . \tag{C4}$$

APPENDIX D: SYMMETRY OF INTERFACE MATRICES

Two configurations in Fig. 12 are transformed into one another by reflection with respect to the interface. This symmetry leads to the relation of the corresponding interface matrices:

$$T_{\xi}(\underline{In}\text{As}\overset{B}{\leftarrow}\text{Ga}\underline{Sb}\overset{A}{}) = \sigma_z T_{\eta}^{-1}(\text{Ga}\underline{Sb}\overset{B}{\leftarrow}\underline{In}\text{As}\overset{A}{})\sigma_z \ , \tag{D1}$$

$$T_{\eta}(\underline{In}\text{As}\leftarrow\text{Ga}\underline{Sb}) = \sigma_z T_{\xi}^{-1}(\text{Ga}\underline{Sb}\leftarrow\underline{In}\text{As})\sigma_z \ , \tag{D2}$$

$$T_z(\underline{In}\text{As}\leftarrow\text{Ga}\underline{Sb}) = \sigma_z T_z^{-1}(\text{Ga}\underline{Sb}\leftarrow\underline{In}\text{As})\sigma_z \ , \tag{D3}$$

where

$$\sigma_z = \begin{bmatrix} 1 & 0 \\ 0 & -1 \end{bmatrix} , \tag{D4}$$

and $T(\underline{In}\text{As}\leftarrow\text{Ga}\underline{Sb})$ represents the interface matrix for the interface atomic configuration $\text{Ga}\underline{Sb}/\underline{In}\text{As}$. The same relation holds between $T(\text{In}\underline{As}\leftarrow\underline{Ga}\text{Sb})$ and $T(\underline{Ga}\text{Sb}\leftarrow\text{In}\underline{As})$.

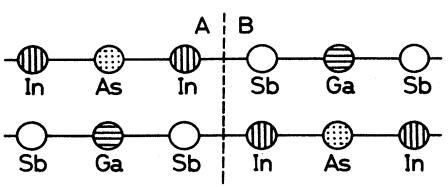

FIG. 12. Symmetry of atomic configurations around the interface of InAs and GaSb.

APPENDIX E: RESULTS IN THE VALENCE-FORCE-FIELD MODEL

With use of the valence-force-field model introduced in Sec. III B, the three-dimensional extension of the bulk dynamical matrix $D_u(\mathbf{k})$ in Eq. (2.3) is written as

$$D_u(\mathbf{k}) = \frac{\omega_{\text{TO}}^2}{r_m + r_m^{-1}} \begin{bmatrix} r_m P(\mathbf{k}) & -Q(\mathbf{k}) \\ -Q(-\mathbf{k}) & r_m^{-1} P(\mathbf{k}) \end{bmatrix} . \tag{E1}$$

Here, the 3×3 matrices $P(\mathbf{k})$ and $Q(\mathbf{k})$ are

$$P(\mathbf{k}) = I + t_2 \begin{bmatrix} f_x & g_{xy} & g_{xz} \\ g_{yx} & f_y & g_{yz} \\ g_{zx} & g_{zy} & f_z \end{bmatrix} , \tag{E2}$$

$$Q(\mathbf{k}) = \begin{bmatrix} b(111) & t_1 b(1\bar{1}\bar{1}) & t_1 b(\bar{1}\,\bar{1}\,1) \\ t_1 b(1\bar{1}\bar{1}) & b(111) & t_1 b(\bar{1}\,1\,\bar{1}) \\ t_1 b(\bar{1}\,\bar{1}\,1) & t_1 b(\bar{1}\,1\,\bar{1}) & b(111) \end{bmatrix} , \tag{E3}$$

where I is a 3×3 unit matrix, and

$$\omega_{\text{TO}}^2 = \frac{4}{3M_r}(F_r + 8F_\theta) \ , \tag{E4}$$

$$t_1 = \frac{F_r - 4F_\theta}{F_r + 8F_\theta}, \quad t_2 = \frac{F_\theta}{F_r + 8F_\theta} \ , \tag{E5}$$

$$f_\alpha = -1 + 2\cos 2k_\beta a_0 \cos 2k_\gamma a_0 - \tfrac{1}{2}\cos 2k_\alpha a_0 (\cos 2k_\beta a_0 + \cos 2k_\gamma a_0) \ , \tag{E6}$$

$$g_{\alpha\beta} = \tfrac{1}{2}\sin 2k_\alpha a_0 \sin 2k_\beta a_0 - i(\cos 2k_\alpha a_0 - \cos 2k_\beta a_0)\sin 2k_\gamma a_0 \ , \tag{E7}$$

$$b(LMN) = \tfrac{1}{4}[e(111) + Le(\bar{1}\,\bar{1}\,1) + Me(1\bar{1}\bar{1}) + Ne(\bar{1}\,1\,\bar{1})] \ , \tag{E8}$$

with $e(lmn) = \exp[i(lk_x + mk_y + nk_z)a_0]$. Subscripts (α,β,γ) are (x,y,z), (y,z,x), or (z,x,y). The symbol $\bar{1}$ means -1.

The parameters appearing in Eq. (3.2) are

$$\begin{aligned} A &= -\nu(1 + 4t_m) \ , \\ B &= -\nu(1 - t_1^2 + 6t_m) \ , \\ C &= -\nu(2t_1 - t_1^2 - 4t_m) \ , \end{aligned} \tag{E9}$$

and the corresponding parameters for acoustic modes are

$$\begin{aligned} A &= \nu(1 + 4t_2) \ , \\ B &= \nu(1 - t_1^2 - 6t_2) \ , \\ C &= \nu(2t_1 - t_1^2 + 4t_2) \ , \end{aligned} \tag{E10}$$

where

$$\nu = \left[\frac{\omega_{\text{TO}}}{r_m + r_m^{-1}} \right]^2 , \quad t_m = \tfrac{1}{2}(r_m^2 + r_m^{-2})t_2 \ . \tag{E11}$$

The relation between envelope functions and displacements is given by

$$\begin{bmatrix}\mathbf{u}_c(\mathbf{k})\\ \mathbf{u}_a(\mathbf{k})\end{bmatrix}=\begin{bmatrix}I & r_m I\\ I & -r_m^{-1}I\end{bmatrix}\begin{bmatrix}I & \Gamma iKa_0\\ \Gamma iKa_0 & I\end{bmatrix}\begin{bmatrix}I & 0\\ 0 & (r_m+r_m^{-1})^{-1}I\end{bmatrix}\begin{bmatrix}\mathbf{U}(\mathbf{k})\\ \mathbf{u}(\mathbf{k})\end{bmatrix}, \tag{E12}$$

where K is defined by Eq. (3.6), and

$$\Gamma=t_1/(r_m+r_m^{-1}) . \tag{E13}$$

The force constants of the linear-chain model (Fig. 4) are

$$F\equiv\frac{f_1}{f_1+f_2}=\begin{cases}\frac{1}{2}(1-t_1) & \text{for } \xi \text{ modes},\\ \frac{1}{2}(1+t_1) & \text{for } \eta \text{ modes},\\ \frac{1}{2} & \text{for } z \text{ modes},\end{cases} \tag{E14}$$

$$F_3\equiv\frac{2f_3}{f_1+f_2}=\begin{cases}-\frac{3}{2}t_2 & \text{for } \xi \text{ modes},\\ -\frac{3}{2}t_2 & \text{for } \eta \text{ modes},\\ t_2 & \text{for } z \text{ modes}.\end{cases} \tag{E15}$$

APPENDIX F: CALCULATION OF INTERFACE MATRICES IN THE PRESENCE OF SECOND-NEIGHBOR FORCES

We show the procedure for calculating interface matrices when we take into account the second-neighbor forces in Fig. 4. From the equations of motion in the vicinity of the interface, we have

$$G_A\begin{bmatrix}u_{aA}(n-1)\\ u_{cA}(n)\\ u_{aA}(n+1)\\ u_{cA}(n+2)\end{bmatrix}=G_B\begin{bmatrix}u_{aB}(n-1)\\ u_{cB}(n)\\ u_{aB}(n+1)\\ u_{cB}(n+2)\end{bmatrix}, \tag{F1}$$

where the 6×6 matrices G_A and G_B are

$$G_A=\begin{bmatrix}f_{3I}-f_{3A} & 0 & f_{3A} & 0\\ 0 & f_{1I}-f_{1A}+f_{3I}-f_{3A} & f_{1A} & f_{3A}\\ f_{3I} & f_{1I} & 0 & 0\\ 0 & f_{3I} & 0 & 0\end{bmatrix}, \tag{F2}$$

$$G_B=\begin{bmatrix}0 & 0 & f_{3I} & 0\\ 0 & 0 & f_{1I} & f_{3I}\\ f_{3B} & f_{1B} & f_{1I}-f_{1B}+f_{3I}-f_{3B} & 0\\ 0 & f_{3B} & 0 & f_{3I}-f_{3B}\end{bmatrix}. \tag{F3}$$

We assume that the force constants f_{1I} and f_{3I} are the average of those for A and B. In the presence of the second-neighbor forces, we have two additional solutions with complex wave numbers. We add only a solution with a decreasing amplitude as it moves away from the interface, called the evanescent wave. The displacements are expressed in terms of the envelope function and the amplitude of evanescent wave χ. For acoustic modes we have

$$\begin{bmatrix}u_a(n-1)\\ u_c(n)\\ u_a(n+1)\\ u_c(n+2)\end{bmatrix}=\begin{bmatrix}1 & -r_m^{-1}\gamma-\frac{3}{2}\\ 1 & r_m\gamma-\frac{1}{2}\\ 1 & -r_m^{-1}\gamma+\frac{1}{2}\\ 1 & r_m\gamma+\frac{3}{2}\end{bmatrix}\begin{bmatrix}U\\ \nabla U\end{bmatrix}+\begin{bmatrix}s/p\\ 1\\ s\\ p\end{bmatrix}\chi . \tag{F4}$$

The quantities p and s are given by the following equation,

$$p+p^{-1}+t+2=0,\quad s=\frac{F_3(2+t/2)+1}{F+(1-F)p^{-1}} , \tag{F5}$$

where $t=-4[F(1-F)+F_3]/F_3^2-4$. We choose a solution of p with $|p|>1$ for A and that with $|p|<1$ for B. For optical modes we have

$$\begin{bmatrix}u_a(n-1)\\ u_c(n)\\ u_a(n+1)\\ u_c(n+2)\end{bmatrix}=\frac{1}{r_+}\begin{bmatrix}-r_m^{-1} & \gamma+\frac{3}{2}r_m^{-1}\\ r_m & \gamma-\frac{1}{2}r_m\\ -r_m^{-1} & \gamma-\frac{1}{2}r_m^{-1}\\ r_m & \gamma+\frac{3}{2}r_m\end{bmatrix}\begin{bmatrix}u\\ \nabla u\end{bmatrix}+\begin{bmatrix}s/p\\ 1\\ s\\ p\end{bmatrix}\chi , \tag{F6}$$

$$s=\frac{F_3(2+t/2)-r_m^{-2}}{F+(1-F)p^{-1}} , \tag{F7}$$

where $t=-2[2F(1-F)-(r_m^2+r_m^{-2})F_3]/F_3^2-4$. Combining the equations, we obtain the following connection rule:

$$\begin{bmatrix}\xi_B\\ \nabla\xi_B\\ \chi_B\\ -\chi_A\end{bmatrix}=\begin{bmatrix}T_{BA}\\ T_{\chi A}\end{bmatrix}\begin{bmatrix}\xi_A\\ \nabla\xi_A\end{bmatrix}, \tag{F8}$$

where the 2×2 matrices T_{BA} and $T_{\chi A}$ cannot be given in an analytical form. The numerical values of T_{BA} are given for InAs/GaSb and GaAs/Ge interfaces in Tables II and III. It is found that the contribution of evanescent waves to the displacements of interface atoms is less than 1%, and the decay length of evanescent waves is about $0.1a$. This indicates that the evanescent waves do not play an important role in the connection rule.

[1]M. V. Klein, IEEE J. Quantum Electron. **QE-22**, 1760 (1986).
[2]J. M. Luttinger and W. Kohn, Phys. Rev. **97**, 869 (1955).
[3]T. Ando and S. Mori, Surf. Sci. **113**, 124 (1982).
[4]G. Bastard, Phys. Rev. B **24**, 5693 (1981).
[5]S. R. White and L. J. Sham, Phys. Rev. Lett. **47**, 879 (1981).
[6]Q.-G. Zhu and H. Kroemer, Phys. Rev. B **27**, 3519 (1983).
[7]M. Altarelli, Phys. Rev. B **28**, 842 (1983).
[8]H. Akera, S. Wakahara, and T. Ando, Surf. Sci. **196**, 694 (1988).
[9]W. Trzeciakowski, Phys. Rev. B **38**, 4322 (1988).
[10]T. Ando and H. Akera, in *Proceedings of the 19th International Conference on the Physics of Semiconductors, Warsaw, 1988,* edited by J. Kossut (Institute of Physics/Polish Academy of Sciences, Warsaw, in press).
[11]R. Tsu and S. S. Jha, Appl. Phys. Lett. **20**, 16 (1972).
[12]A. S. Barker, Jr., J. L. Merz, and A. C. Gossard, Phys. Rev. B **17**, 3181 (1978).
[13]A. Fasolino, E. Molinari, and J. C. Maan, Phys. Rev. B **33**, 8889 (1986).
[14]A. Fasolino, E. Molinari, and J. C. Maan, Superlatt. Microstruct. **3**, 117 (1987).
[15]A. Fasolino, E. Molinari, and J. C. Maan, Phys. Rev. B **39**, 3923 (1989).
[16]E. Richter and D. Strauch, Solid State Commun. **64**, 867 (1987).
[17]S. F. Ren, H. Chu, and Y. C. Chang, Phys. Rev. Lett. **59**, 1841 (1987); Phys. Rev. B **37**, 8899 (1988).
[18]T. Tsuchiya, H. Akera, and T. Ando, Phys. Rev. B **39**, 6025 (1989).
[19]S. M. Rytov, Zh. Eksp. Teor. Fiz. **29**, 605 (1955) [Sov. Phys.—JETP **2**, 466 (1956)].
[20]E. P. Pokatilov and S. I. Beril, Phys. Status Solidi B **110**, K75 (1982); **118**, 567 (1983).
[21]R. E. Camley and D. L. Mills, Phys. Rev. B **29**, 1695 (1984).
[22]L. Wendler, Phys. Status Solidi B **129**, 513 (1985).
[23]R. Fuchs and K. L. Kliewer, Phys. Rev. **140**, A2076 (1965).
[24]A. A. Lucas, E. Kartheuser, and R. G. Badro, Phys. Rev. B **2**, 2488 (1970).
[25]J. J. Licari and R. Evrard, Phys. Rev. B **15**, 2254 (1977).
[26]D. L. Mills, Vijnana Parishad Anusandhan Patrika **14**, 115 (1971).
[27]M. Babiker, J. Phys. C **19**, 683 (1986).
[28]H. Chu, S. F. Ren, and Y. C. Chang, Phys. Rev. B **37**, 10 746 (1988).
[29]S. M. Rytov, Akust. Zh. **2**, 71 (1956) [Sov. Phys.—Acoust. **2**, 67 (1956)].
[30]Preliminary work is presented in Ref. 8.
[31]M. Born and K. Huang, *Dynamical Theory of Crystal Lattices* (Oxford University Press, Oxford, 1954).
[32]M. J. P. Musgrave and J. A. Pople, Proc. R. Soc. London, Ser. A **268**, 474 (1962).
[33]H. Bilz and W. Kress, *Phonon Dispersion Relations in Insulators* (Springer-Verlag, Berlin, 1979).
[34]B. Jusserand and D. Paquet, Phys. Rev. Lett. **56**, 1752 (1986).
[35]S. K. Yip and Y. C. Chang, Phys. Rev. B **30**, 7037 (1984).
[36]E. Molinari, A. Fasolino, and K. Kunc. Phys. Rev. Lett. **56**, 1751 (1986).
[37]E. Molinari, A. Fasolino, and K. Kunc, in *Proceedings of the 18th International Conference on the Physics of Semiconductors, Stockholm, 1986,* edited by O. Engström (World Scientific, Singapore, 1987), Vol. 1, p. 663.
[38]C. Colvard, T. A. Gant, M. V. Klein, R. Merlin, R. Fischer, H. Morkoç, and A. C. Gossard, Phys. Rev. B **31**, 2080 (1985).
[39]A. K. Sood, J. Menéndez, M. Cardona, and K. Ploog, Phys. Rev. Lett. **54**, 2111 (1985).
[40]A. K. Sood, J. Menéndez, M. Cardona, and K. Ploog, Phys. Rev. Lett. **56**, 1753 (1986).
[41]A. Ishibashi, M. Itabashi, Y. Mori, K. Kaneko, S. Kawado, and N. Watanabe, Phys. Rev. B **33**, 2887 (1986).
[42]Z. P. Wang, D. S. Jiang, and K. Ploog, Solid State Commun. **65**, 661 (1988).
[43]R. Lassnig, Phys. Rev. B **30**, 7132 (1984).
[44]M. H. Degani and O. Hipólito, Phys. Rev. B **35**, 7717 (1987); Surf. Sci. **196**, 459 (1988).
[45]L. Wendler and R. Pechstedt, Phys. Rev. B **35**, 5887 (1987).
[46]P. Brüesch, *Phonons: Theory and Experiments II* (Springer-Verlag, Berlin, 1986).